(4)

The University of Texas at Dallas
Center for Quantum Electronics
The Gamma-Ray Laser Project
Quarterly Report
October-December 1988

Report GRL/8803

PROOF OF THE FEASIBILITY OF COHERENT AND INCOHERENT SCHEMES FOR PUMPING A GAMMA-RAY LASER

Principal Investigator: Carl B. Collins
The University of Texas at Dallas
Center for Quantum Electronics
P. O. Box 830688
Richardson, Texas 75083-0688

January 1989

Quarterly Technical Progress Report
1 October 1988 through 31 December 1988
Contract Number N00014-86-C-2488

Prepared for
INNOVATIVE SCIENCE AND TECHNOLOGY DIRECTORATE
OF STRATEGIC DEFENSE INITIATIVE ORGANIZATION

Contracting Officer's Technical Representative
Dr. Paul Kepple, Code 4720
Naval Research Laboratory
4555 Overlook Avenue, SW
Washington, DC 20375-5000

SECURITY CLASSIFICATION OF THIS PAGE (When Data Entered)

REPORT DOCUMENTATION PAGE

READ INSTRUCTIONS BEFORE COMPLETING FORM

1. REPORT NUMBER: GRL/8803	2. GOVT ACCESSION NO.
3. RECIPIENT'S CATALOG NUMBER	
4. TITLE (and Subtitle): PROOF OF THE FEASIBILITY OF COHERENT AND INCOHERENT SCHEMES FOR PUMPING A GAMMA-RAY LASER	5. TYPE OF REPORT & PERIOD COVERED: Quarterly Technical Progress 10/01/88 - 12/31/88
	6. PERFORMING ORG. REPORT NUMBER
7. AUTHOR(s): C. B. Collins	8. CONTRACT OR GRANT NUMBER(s): N00014-86-C-2488
9. PERFORMING ORGANIZATION NAME AND ADDRESS: University of Texas at Dallas, Center for Quantum Electronics, P. O. Box 830688, Richardson, TX 75083-0688	10. PROGRAM ELEMENT, PROJECT, TASK AREA & WORK UNIT NUMBERS
11. CONTROLLING OFFICE NAME AND ADDRESS: INNOVATIVE SCIENCE AND TECHNOLOGY DIRECTORATE OF STRATEGIC DEFENSE INITIATIVE ORGANIZATION	12. REPORT DATE: January 1989
	13. NUMBER OF PAGES: 71
14. MONITORING AGENCY NAME & ADDRESS (if different from Controlling Office): Dr. Paul Kepple, Code 4720, Naval Research Laboratory, 4555 Overlook Avenue, SW, Washington, DC 20375-5000	15. SECURITY CLASS. (of this report): Unclassified
	15a. DECLASSIFICATION/DOWNGRADING SCHEDULE

16. DISTRIBUTION STATEMENT (of this Report)

This document has been approved for public release and sale; its distribution is unlimited.

17. DISTRIBUTION STATEMENT (of the abstract entered in Block 20, if different from Report)

18. SUPPLEMENTARY NOTES

19. KEY WORDS (Continue on reverse side if necessary and identify by block number)

20. ABSTRACT (Continue on reverse side if necessary and identify by block number)

Recent approaches to the problem of the gamma-ray laser have focused upon upconversion techniques in which metastable nuclei are pumped with long wavelength radiation. At the nuclear level the storage of energy can approach tera-Joules (10^{12} J) per liter for thousands of years. However, any plan to use such a resource
(continued on next page)

DD FORM 1 JAN 73 1473 EDITION OF 1 NOV 65 IS OBSOLETE

SECURITY CLASSIFICATION OF THIS PAGE (When Data Entered)

20. ABSTRACT (continued)

for a gamma-ray laser poses problems of a broad interdisciplinary nature requiring the fusion of concepts taken from relatively unrelated fields of physics. Our research group has described several means through which this energy might be coupled to the radiation fields with cross sections for stimulated emission that could reach 10^{-17} cm^2. Such a stimulated release could lead to output powers as great as 3×10^{21} Watts/liter. Since 1978 we have pursued an approach for the upconversion of longer wavelength radiation incident upon isomeric nuclear populations that can avoid many of the difficulties encountered with traditional concepts of single photon pumping. Recent experiments have confirmed the general feasibility and have indicated that a gamma-ray laser is feasible if the right combination of energy levels and branching ratios exists in some real material. Of the 1,886 distinguishable nuclear materials, the present state-of-the-art has been adequate to identify 29 first-class candidates, but further evaluation cannot proceed without remeasurements of nuclear properties with higher precision. A laser-grade database of nuclear properties does not yet exist, but the techniques for constructing one have been developed under this contract and are now being utilized. Resolution of the question of the feasibility of a gamma-ray laser now rests upon the determination of: 1) the identity of the best candidate, 2) the threshold level of laser output, and 3) the upconversion driver for that material.

This quarter's report focuses upon the continued success enjoyed along the approach to the gamma-ray laser that depends upon incoherent pumping. This nuclear analog of the ruby laser embodies the simplest concept for a gamma-ray laser and it is not surprising that the greatest rate of achievement toward a sub-Angstrom laser has continued in that direction. Emphasis has remained upon the systematics of the discovery of giant pumping resonances that enabled us to dump populations of the only available sample of the 29 candidates, $^{180}Ta^m$, through a cross section that was 10,000 times more favorable than even the most optimistic estimates. The lessons taught by that major milestone have been extended throughout the region of mass-180 nuclides. Reported this quarter is success in pumping the difficult isotope, ^{176}Lu, to find an enormous integrated cross section of 4.1×10^{-22} cm^2 eV for the reaction $^{176}Lu(\gamma,\gamma')^{176}Lu^m$. This result effectively completes the validation of the systematics for the occurrence of these giant pumping resonances in the mass-180 region bounded by ^{167}Er and ^{191}Ir. *Only one nucleus in this region has been found to have an isomer of detectable lifetime and no giant resonance for pumping it.* The significance of this result is that some of the better candidates for a gamma-ray laser lie in this mass region.

TABLE OF CONTENTS

PREFACE

Emphasis this quarter returns to the successes enjoyed along the approach to the gamma-ray laser that depends upon incoherent pumping. There is embodied the very simplest concept for a gamma-ray laser and it is no surprise that the greatest rate of achievement has continued in that direction.

Receiving first attention is a report of continued success in extending the lessons taught by $^{180}Ta^{m}$ throughout the A = 180 mass region where lie some of the better of the 29 candidate materials for a gamma-ray laser. Last year we reported the giant resonance for the dumping of the $^{180}Ta^{m}$ isomer by pumping samples with flash x-rays of relatively modest intensities in a scheme which is the nuclear analog of the ruby laser. This particular material, the worst of the 29 actual candidates, showed what was at that time the largest integrated cross section ever reported for interband transfer in any nuclear material, 4 x 10^{-22} cm^2 eV. This is an enormous value for bandwidth funneling to a fluorescent level, corresponding to about 0.5 eV of useful width for the absorption of the pump x-rays. Subsequent studies showed that these giant pumping resonances occurred with a gratifying frequency throughout the table of nuclides. However, the very largest values of integrated cross section were found to be concentrated in the mass-180 region bounded by ^{167}Er and ^{191}Ir. *Only one nucleus in this region has been found to have an isomer of detectable lifetime and no giant resonance for pumping it.*

This quarter we present further confirmation of favorable systematics in the 180 region with the report of an integrated cross section of 4.1 x 10^{-22} cm^2 eV for the reaction $^{176}Lu(\gamma,\gamma')^{176}Lu^{m}$. A particularly difficult species, this material had not been previously attempted in our project and the success reported here is particularly welcome in providing systematic completeness. *As usual with these experiments, no significant contributions were made by spurious neutrons evaporated from environmental materials.*

The nuclide ^{176}Lu has astrophysical significance, as well, and the importance of the giant pumping resonance to those concerns is reported in a separate section as a matter of interest.

Finally, in this report is discussed our continued progress in extending the technologies we introduced for the calibration of intense bremsstrahlung sources to machines with end point energies above 1.5

MeV. Then follows a study of the utility of the Compton scattering of bremsstrahlung pulses in order to produce source spectra with variable end point energies.

As has been the case since 1982, there are still no known factors which inhibit the realization of a gamma-ray laser. Neither the level of pump fluence required for laser threshold nor the waste heat to reject presents any particular problem in idealized materials. *A gamma-ray laser is feasible if the right combination of energy levels occurs in some real material.* When actually tested, the two poorest of the 29 candidate nuclei did surprisingly well, performing 1,000 to 10,000 times better than expected. The overriding question in resolving the feasibility of the nuclear analog to the ruby laser is whether or not one of the better of the 29 has its isomeric level in a position sufficiently near the ideal.

Continuing the preparation of this report as an "in-house" journal, this series presents material to reflect the individual contributions of the teams of research faculty and graduate students involved in these phases of the research. In this regard, I wish to thank all our staff for their splendid efforts in supporting the preparation of these manuscripts to a rather demanding timetable.

- C. B. Collins
- Director
- Center for Quantum Electronics

DETERMINATION OF PHOTOEXCITATION CROSS SECTIONS FOR $^{176}Lu(\gamma,\gamma')\ ^{176}Lu^{m}$ USING A 6 MeV BREMSSTRAHLUNG SOURCE

by J. A. Anderson, K. N. Taylor, J. J. Carroll, M. J. Byrd, and C. B. Collins
Center for Quantum Electronics, University of Texas at Dallas
E. C. Scarbrough and P. P. Antich
University of Texas Southwestern Medical Center

Introduction

The isomer $^{176}Lu^{m}$ is of intrinsic interest in nuclear photoactivation studies because of its proximity in the chart of nuclides to other isomeric nuclei, such as ^{167}Er, ^{179}Hf, ^{180}Ta, and ^{191}Ir, which have been found[1,2,3,4] to manifest very large (γ,γ') cross sections in the range below 6 MeV. The mechanisms for populating the isomeric state in this nuclide are also of interest for astrophysical applications, since the long half-life of the ground state ^{176}Lu (3.6×10^{10} y) makes it a candidate for use as an astrophysical chronometer. Several investigators[5,6,7] have recently studied it for this purpose. However, the existence of the relatively short-lived isomeric state $^{176}Lu^{m}$ (E = 126 keV, $T_{1/2}$ = 3.68 h), which beta decays to form ^{176}Hf, complicates this scheme. Because of this state, photoexcitation of the isomer could prematurely bleed away the ground state population and invalidate the operation of the chronometer. The work described here is concerned with determining the size of the transfer cross section for the reaction $^{176}Lu(\gamma,\gamma')^{176}Lu^{m}$ by using a bremsstrahlung source with a fixed endpoint near 6 MeV. A separate paper[8] considers the astrophysical implications of these experiments.

Because of the very narrow linewidths associated with long-lived, isomeric nuclear states, the cross sections for directly exciting these states by photoabsorption are quite small. However, the cross sections for isomeric excitation via a cascade from higher-lying intermediate states can be many orders of magnitude greater than those for the direct process. This mechanism has previously been discussed in Refs. 1-4.

The resulting total activation, N_e, of an irradiated sample can be described by

$$N_e = N_T \sum_i [\pi b_a b_o \sigma_o \Gamma/2]_i \, \Phi(E_i) \quad , \qquad (1)$$

where N_T is the number of target nuclei in the sample, the quantity in square brackets is the effective integrated cross section for transfer through the ith gateway state, Φ_i is the time-integrated, incident photon flux at the energy E_i of the ith gateway, and the summation is taken over all accessible gateways. The terms appearing in the integrated cross section are the Breit-Wigner cross section, σ_o, the width of the resonance, Γ, and the branching ratios from the gateway state to the ground and excited states, b_a and b_o. The units of the integrated transfer cross section are cm^2-keV; the units for the time-integrated photon flux are photons/(cm^2-keV).

For the case of $^{176}Lu^m$, at least one intermediate gateway state has been observed by Norman et al.[5] in the energy range between 661 keV and 1332 keV. In that work, lutetium samples were exposed to radiation from medical irradiation machines using both ^{137}Cs and ^{60}Co sources. They found that the isomeric level was photoactivated slightly by the ^{60}Co source (E_{max} = 1332 keV), but not by the ^{137}Cs source (E_{max} = 662 keV). Because of the extended nature of the source and shielding configurations in these devices, the gamma-ray spectra in such cases are not simple line spectra, but show broad continua on the low energy side of the line(s) due to the radiation transport process.[9] Unfortunately, Norman et al. did not use the real spectral distribution from the irradiation source. Moreover, they analyzed their results as if the photoabsorption process were a bound-free transition with a threshold rather than treating the case of bound-bound transitions that would actually hold in this energy range. Without an accurate knowledge of the spectral intensity function for the irradiation source and of the energy of the gateway state, it is not possible to determine the integrated cross section for transfer into the isomeric state.

The study described here has approached the source definition problem by using a relatively well characterized bremsstrahlung source,[10] the Varian CLINAC 1800 operated in the 6 MeV mode. The spectrum from this device is shown in Fig. 1. By measuring the total activation obtained during an exposure and employing the relative

intensity information contained in Fig. 1, it is possible to generate a plot of integrated cross section as a funtion of tne energy assumed for a single gateway. The results of the current study are presented in this form.

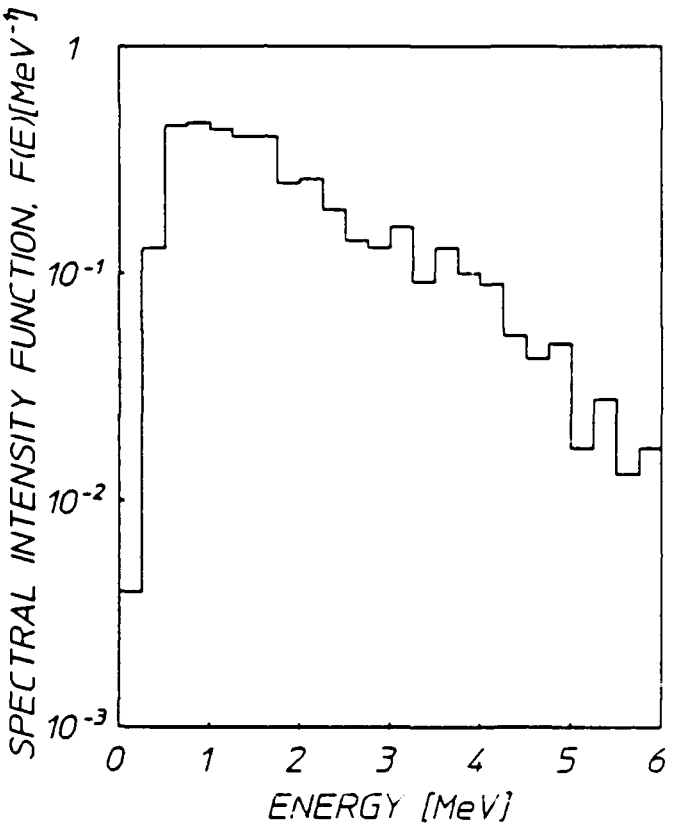

Figure 1: Spectral intensity for the Varian CLINAC 1800 operated in the 6 MeV mode. The curve has been normalized to represent a single incident photon. Actual photon fluxes were obtained from this information by dividing the measured dose by the dose-per-photon calculated on the basis of this intensity distribution.

Detection of the isomeric state $^{176}Lu^{m}$ once it has been created presents some difficulties. A partial energy level diagram[11] showing $^{176}Lu^{m}$ and its beta-decay daughter product, ^{176}Hf, is shown in Fig. 2. The long-lived ground state decays principally (99.1%) to the state lying at 597 keV in ^{176}Hf. The characteristic signature of this decay is

a beta-particle with an endpoint of 565 keV and major gamma rays at 88.4 keV (13.1% intensity), 201.9 keV (84%), and 306.9 keV (93%). Photoexcitation of the isomer is indicated as proceeding through an as yet uncharacterized intermediate state. The isomer decays wholly by beta decay, with 39.6% of the decays terminating on the ground state in ^{176}Hf and having a beta decay endpoint energy of 1313 keV. The other 60.4% of the decays terminate on the ^{176}Hf state at 88.4 keV, have an endpoint energy of 1225 keV, and are accompanied by several low intensity gamma rays. The most prominent of these gamma rays is the 88.4 keV line, which has an intensity of 8.9%. Thus, detection schemes for the isomer which are based on gamma-ray counting must utilize the 88.4 keV line, which suffers strong interference from the ground state ^{176}Lu decay.

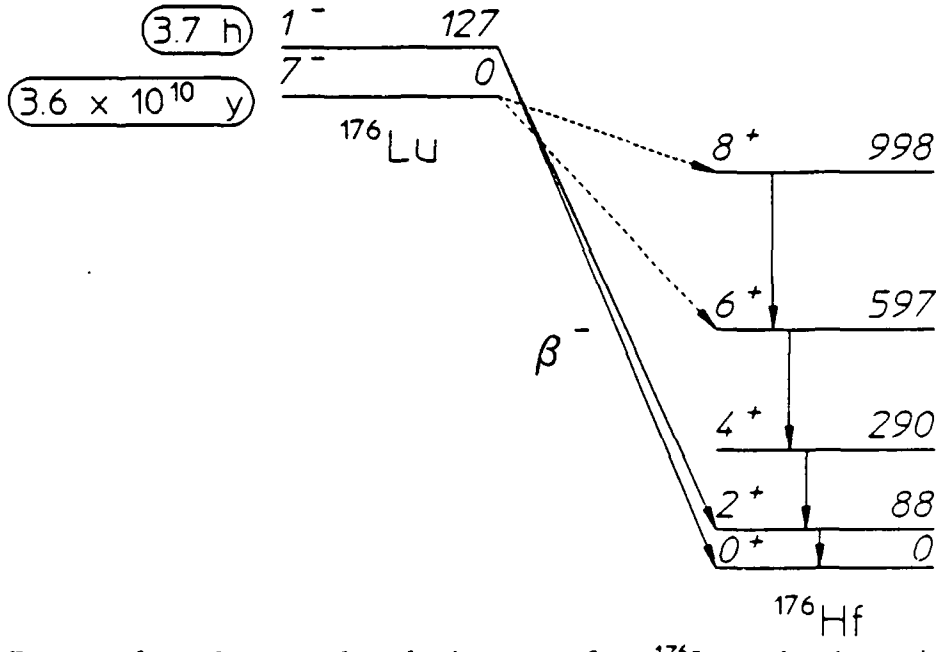

Figure 2: Energy level diagram for ^{176}Lu, showing the beta decay of the isomeric state to ^{176}Hf. The advantage of the Cerenkov detection scheme used in this work is that the beta particles from decay of the isomeric state can be cleanly separated from those resulting from decay of the ground state.

An alternative approach to gamma-ray counting is to directly detect the beta particles emitted during the decay process. This can be done either by standard liquid scintillation counting, or, because of the high end-point energy of the decay, by counting Cerenkov photons generated by the passage of the beta particles through the sample

solvent. Both processes offer high net efficiencies compared to the gamma-ray counting technique, but the Cerenkov method has the additional advantage of being relatively insensitive to interference from the lower energy beta particles emitted by the decay of the ground state. The threshold for production of Cerenkov radiation by beta particles passing through a medium is given by[12]

$$E_{th} = m_0c^2\{-1 + [n^2/(n^2-1)]^{1/2}\} \quad , \qquad (2)$$

where n is the index of refraction of the medium and m_ec^2 is the 511 keV rest mass energy of the electron. Thus, for water (n = 1.33) no Cerenkov radiation will be emitted for electrons with energies less than about 260 keV. Above threshold, the efficiency for the production of Cerenkov photons in water rises steeply, being about eight times greater at 1000 keV than it is at 500 keV.[13] The net result of these two effects is to make the Cerenkov detector almost blind to the steady background generated by the decay of the ^{176}Lu ground state. Since the Cerenkov process causes many photons to be emitted as the electron is slowed down, background contributions due to photomultiplier noise can also be suppressed by using a coincidence counting technique.

Experimental Detail

The samples used for this work consisted of a nominal 5 grams of lutetium chloride ($LuCl_3 \cdot 6H_2O$) dissolved in water to produce approximately 20 ml of solution. Table I lists sample weights and other pertinent parameters. Samples were held in standard 20 ml polyethylene scintillation vials obtained from Research Products Incorporated.

Table I: Sample parameters for the Cerenkov counter experiments. N_T is the number of target ^{176}Lu nuclei in the sample. The natural abundance of ^{176}Lu was taken to be 2.59%[14].

Sample ID	Mass, $LuCl_3 \cdot (6H_2O)$ [g]	N_T
I	4.993	2.00×10^{20}
III	4.971	1.99×10^{20}

A simple coincidence counter was constructed using two RCA 8850 photomultipliers mounted on a common axis in E. G. & G. 9201 tube bases. A special lightproof fixture held the scintillation vials centered between the two photomultipliers. The fast (approximately 6 ns) outputs from these tubes were amplified, time synchronized, and input to a discriminator in order to produce logic pulses which could drive a 150 MHz logic unit (Phillips Model 755). The output from the logic unit could be accumulated on either a simple counter or a multichannel scaler (MCS). A schematic diagram of the data acquisition system is shown in Fig. 3.

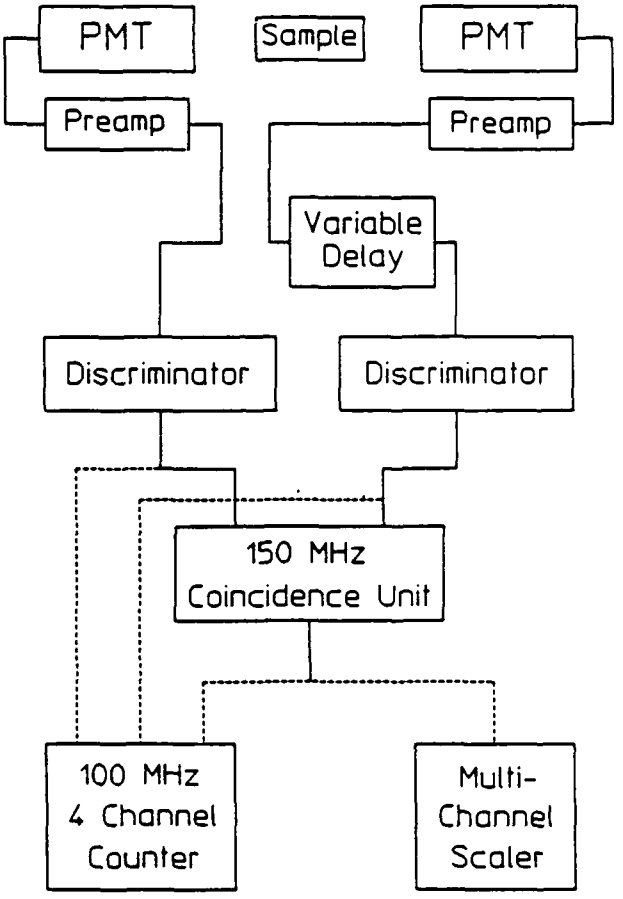

Figure 3: Data acquisition system for the Cerenkov counter used in this work. Coincidence circuitry was used to suppress dark noise in the photomultipliers since counting rates in the experiment were less than 10 counts/s.

Because the efficiency of a Cerenkov counter varies strongly with the endpoint energy of the beta decay being monitored, it is necessary to use a calibration standard having essentially the same endpoint as the nuclide to be counted. As noted above, the endpoints of the beta decay channels from the isomer are 1225 keV and 1313 keV, with a weighted average of 1260 keV. Naturally occurring radioactive ^{40}K has a beta endpoint energy of 1330 keV, and for reasons of convenience was chosen as the calibration standard for this work. Calibration standards with nominal amounts of 1, 2, 3, 4, and 5 grams of KCl dissolved in

water to make 20 ml of sample were prepared and were placed in counting vials. These vials were counted before each run to determine the detector efficiency for the particular choice of discriminator settings, PMT voltages, etc. used in a given experiment. The net counting efficiency was found to lie in the range 10.3-13.6%.

Three different sample exposures, each of about 40 minutes, were made. The samples were oriented with the cylindrical axis of the sample vial perpendicular to the x-ray beam axis. The vials were located 63.7 cm from the x-ray converter. At this position, the total dose delivered to the sample was about 44.2 kRad during a 40 minute exposure. Table II lists the exposure times, sample identifications, and counting times for the different exposures.

Table II: Exposure and counting conditions for $^{176}Lu^{m}$ excitation. Transit time is the time elapsed between the end of the irradiation and the start of the counting measurement. Effective dwell time is the dwell time obtained after collapsing the number of channels in the MCS spectrum; the actual MCS dwell time was typically 40 s.

Exposure	Sample ID	Exposure Time [s]	Transit Time [s]	Effective Dwell Time [s]
1	I	2805	2955	320
2	I	2400	3165	320
3	III	1799	3315	320

Analysis

In the first experiment, a significant amount of activation was observed following the irradiation, as shown in the multichannel spectrum of Fig. 4. As can be seen from the figure, the principal decay component observed has a half-life of 3.83 ± 0.05 h, in reasonable

agreement with the accepted value of 3.68 h for $^{176}Lu^{m}$. This value was obtained by fitting a line to the log of the number of counts per channel, after correction for background, for data between t = 20070 s and t = 60070 s. Here, t is the time elapsed after the end of the irradiation.

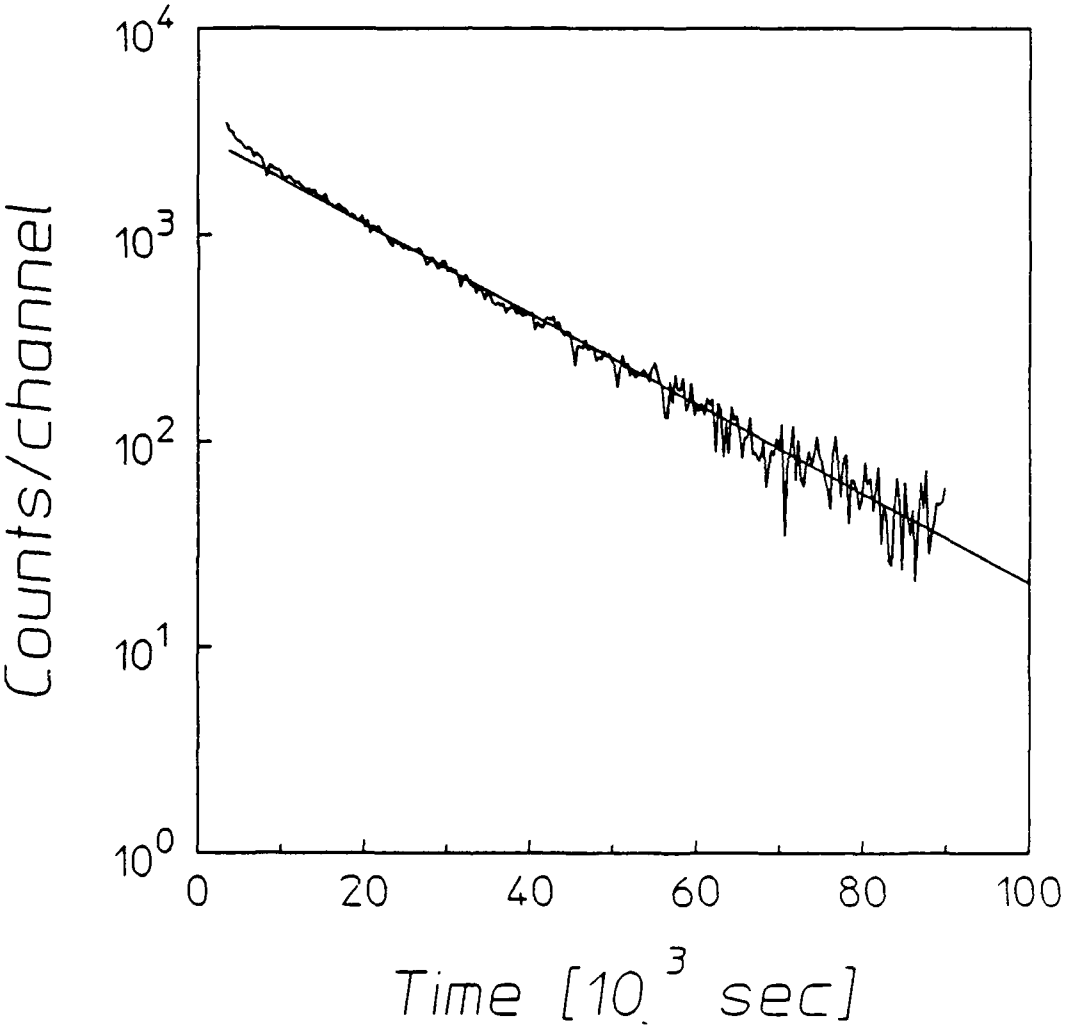

Figure 4: Decay spectrum for trial 1. Here, and in Figs. 5 and 6, the number of background-corrected counts per channel of the multichannel scaler are plotted vs. the time since the end of the irradiation. The spectrum shows the superposition of the $^{176}Lu^{m}$ decay and the thermoluminescence decay from the polyethylene bottle. The line fitted to the data corresponds to a half-life of 3.83 h.

A second component with a faster decay is also clearly present at early times in the MCS spectrum of Fig. 4. Subsequent experiments in which the bottle, the fluid, and the bottle cap were separately counted identified the source of this fast component as count-rate generated coincidences from single-photon thermoluminescence phenomena arising in the polyethylene bottle. In these secondary experiments, a sample was irradiated and then broken apart into its components (cap, bottle, fluid). From these components and from pristine, non-irradiated parts, three samples, which were identical except for the choice of the irradiated component, were created. These samples were then counted to unambiguously identify the source of the fast decay component. It was found that the phenomena was present regardless of whether the fluid was the $LuCl_3$ solution or pure water. Examination of the count-rates from the individual photomultipliers indicated that the fast component was due to accidental coincidences between independent, random events occurring on the two detector channels when the irradiated polyethylene bottle was counted. Further experiments demonstrated that the fast decay component could be either "stored" by cooling the bottle with liquid nitrogen or quenched by heating the bottle, thus identifying the process as some type of radiation-induced thermoluminescence.

A second run, made after the fast decay component had been identified and steps were taken to remove it, yielded a half-life value of 3.58 ± 0.05 h for the lutetium activation. The data between t = 3325 s and t = 32125 s were fit to obtain this result. These data are shown in Fig. 5. However, the intensity of the observed Cerenkov radiation was much less in this second case. This decrease in intensity was traced to the deterioration of the cap on the scintillation vial and an attendant buildup of readily visible debris suspended in the lutetium solution. A third and final run made with a freshly prepared sample is shown in Fig. 6. It yielded a value of 3.57 ± 0.04 h for the half-life when a fit was made to the data between t = 3795 s and t = 60115 s. The average value for the half-life obtained from these experiments is therefore 3.66 ± 0.08 h, in good agreement with the literature value.

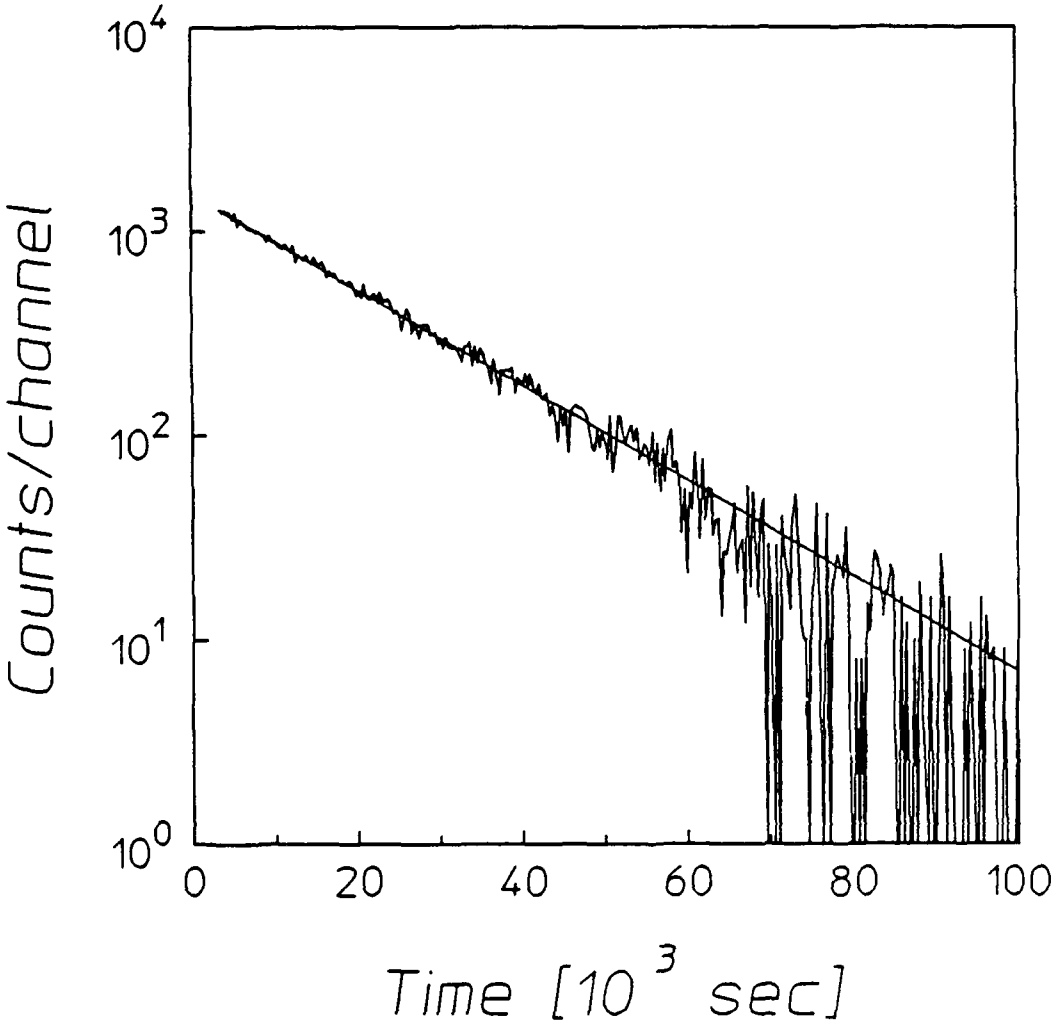

Figure 5: Decay spectrum for trial 2. The thermoluminescence contribution was removed by quenching the bottle in hot water before counting. The reduced intensity of this data set compared to Trials 1 and 3 was traced to suspended debris in the counting solution. The line fitted to the curve corresponds to a half-life of 3.58 h.

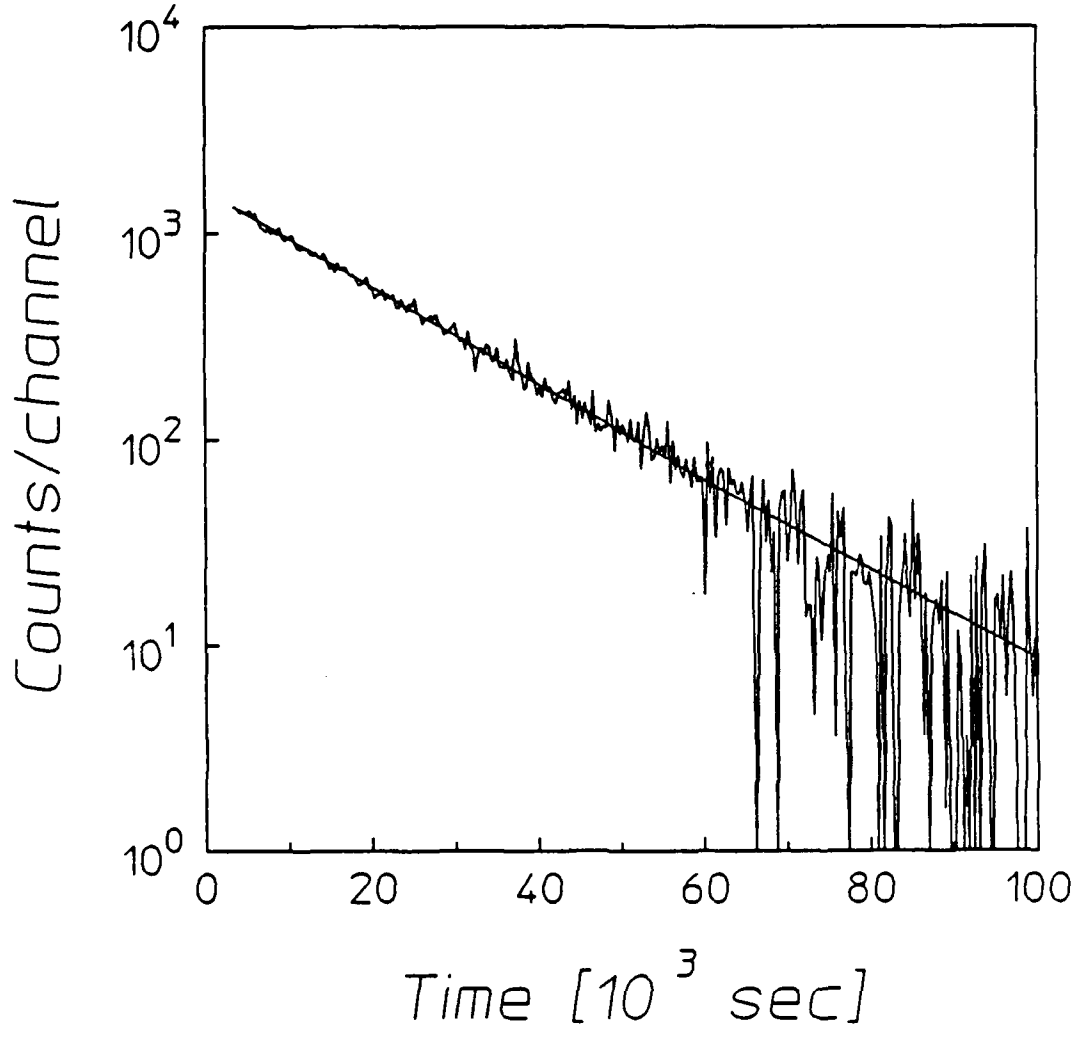

Figure 6: Decay spectrum for trial 3. The thermoluminescence contribution was removed by transferring the counting solution to an unirradiated bottle. The half-life of the fitted curve is 3.57 h.

The fits to the experimental data for the number of net counts in a channel, C, were of the form

$$C = (C_{obs} - C_{bkg}) = C_o e^{-\lambda t} \quad , \qquad (3)$$

where C_{obs} is the number of counts observed in a channel of the multi-channel scaler spectrum and C_{bkg} is the number of counts in the channel due to background. In Eq. (3), the number of counts per channel immediately after the irradiation, C_o, and the decay constant, k, are

the fitted parameters. The decay constant is related to the half-life, $T_{1/2}$, by $\lambda = \ln(2)/T_{1/2}$. The net activity, A_o, for the sample at the end of the irradiation can then be obtained from

$$A_o = \frac{C_o}{\eta f t_d} \quad , \tag{4}$$

where η is the efficiency of the counter, f is the branching ratio for the beta decay (100% in this case), and t_d is the dwell time for the MCS spectrum. By using the general relationship between the activity of a sample and the number of radioactive nuclei in it, one can calculate the number of excited nuclei in the sample at the end of the irradiation, $N_{e,o}$, from

$$N_{e,o} = \frac{A_o}{\lambda} \quad . \tag{5}$$

Finally, the total number of excitations induced by the exposure, N_e, will be somewhat larger than this because of decays which occurred during the irradiation. The correction takes the form

$$N_e = N_{e,o} \times \frac{\lambda t_e}{(1-e^{-(\lambda t_e)})} \quad , \tag{6}$$

where t_e is the exposure period.

The integrated cross section, $\sigma\Gamma$, is related to the number of excited nuclei by

$$\sigma\Gamma = \frac{N_e}{N_T \phi(E) t_e} \quad , \tag{7}$$

where N_T is the number of target nuclei in the sample and $\phi(E)$ is the photon flux, expressed in photons/(cm^2-keV-s) at the energy of the gateway state. In this expression, $\phi(E)t_e$ has replaced the integrated photon flux Φ appearing in Eq. (1). As noted above, the energy of the gateway state (or states) is unknown in this case. Therefore, a single gateway will be assumed and the results will be presented in the form of a plot of cross section as a function of the possible values of this

gateway state. For the purpose of initially calculating the cross sections, the flux at an assumed gateway of 2.125 MeV will be used; the cross sections at other energies are obtained by multiplying this by a factor expressing the relative intensities shown in Fig. 1.

The fits to the experimental data of Figs. 4 and 6 yielded values for C_o of 3022 and 1619 counts. Use of the fitted values for λ and the appropriate efficiencies and exposure times indicated that 1.48×10^6 and 8.96×10^5 excited nuclei were produced in trials 1 and 3. trial 2 was not considered in this analysis because of the sample contamination problem discussed above. One further correction, not discussed above, is required to account for interferences from neutron capture processes that populate the isomeric state through the reaction $^{175}Lu(n,\gamma)^{176}Lu^m$. The natural abundance of the parent species in this reaction is 97.41%. In a previous study[1], the thermal and epithermal neutron fluxes at the sample position were found to be ϕ_{therm} = 12 n/(cm^2-s) and ϕ_{epi} = 6 n/(cm^2-s). Using these fluxes and the cross sections for populating the isomer through the capture process (σ_{therm} = 16 barns and σ_{epi} = 550 barns)[15], the number of excited nuclei produced by neutron capture, $N_{e,n}$, can be calculated from

$$N_{e,n} = N_{T'}[\phi_{therm}\sigma_{therm} + \phi_{epi}\sigma_{epi}]t_e \quad , \qquad (8)$$

where $N_{T'}$ is the number of ^{175}Lu nuclei in the sample. Before the photoactivation cross sections were calculated, the neutron contamination from this source was subtracted from the values of N_e cited above . Because of the large epithermal cross section and the high natural abundance of the parent nuclide, the neutron capture contribution is considerably larger than those seen in the previous study. It amounts to approximately 5% of the total number of excited nuclei observed in these experiments.

At a distance of 63.7 cm from the x-ray source, the photon intensity at 2.125 MeV was 5.94×10^6 photons/(cm^2-keV-s). From this intensity, integrated cross sections of 39.9×10^{-26} and 42.2×10^{-26} cm^2-keV were calculated using the corrected values for the number of excited nuclei produced in trials 1 and 3. The average of these two measurements,

$$[\sigma\Gamma](E = 2.125 \text{ MeV}) = 41.0 \times 10^{-26} \text{ cm}^2\text{-keV} \quad , \qquad (9)$$

is taken to be the experimental result for the cross section for an assumed gateway at 2.125 MeV. A plot of integrated cross section vs. the energy of the hypothetical single gateway state is shown in Fig. 7.

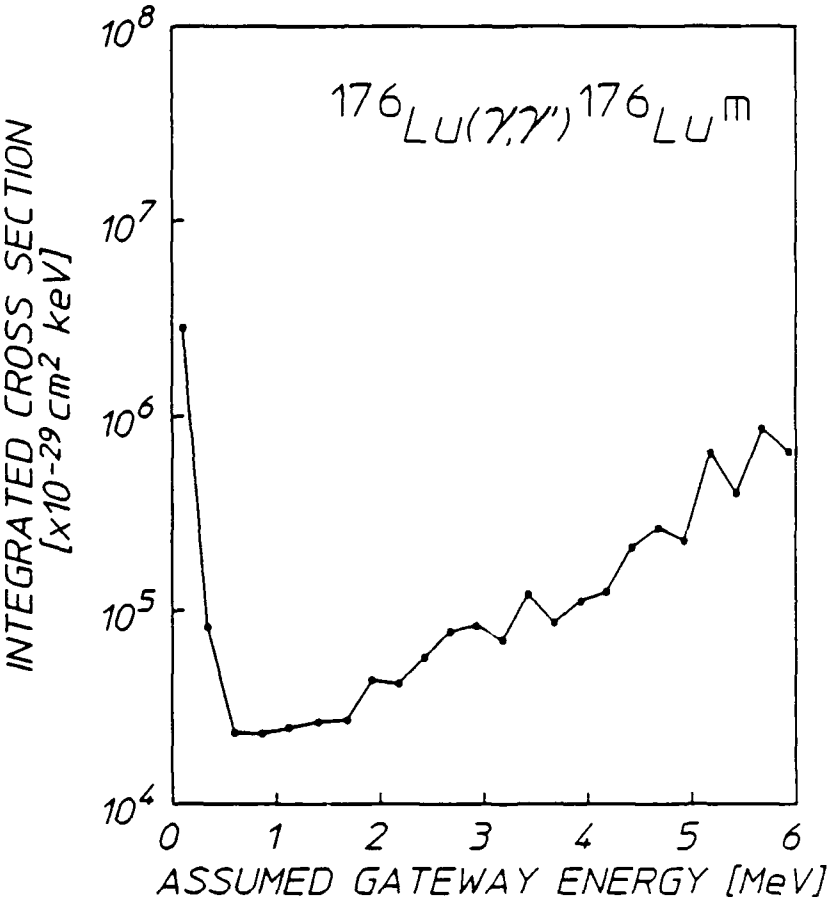

Figure 7. Integrated cross section for the reaction $^{176}Lu(\gamma,\gamma')^{176}Lu^{m}$ as a function of the assumed gateway energy.

Discussion

The cross section we have obtained for the process $^{176}Lu(\gamma,\gamma')^{176}Lu^{m}$ is comparable to those obtained for other materials[1] in this region of the nuclide chart. Assuming for the sake of comparison that the gateway energies are all about 2.125 MeV, the value given above is commensurate with those obtained for ^{167}Er ($\sigma\Gamma$ = 43 × 10^{-26} cm^2-keV), ^{179}Hf ($\sigma\Gamma$ = 31 × 10^{-26} cm^2-keV), $^{180}Ta^{m}$ ($\sigma\Gamma$ = 49 × 10^{-26} cm^2-keV), ^{191}Ir ($\sigma\Gamma$ = 41 × 10^{-26} cm^2-keV), ^{195}Pt ($\sigma\Gamma$ = 21 × 10^{-26} cm^2-keV), and ^{197}Au ($\sigma\Gamma$ = 15 × 10^{-26}

cm^2-keV). Only two of the materials tested in this mass region have exhibited substantially lower cross sections under the assumption of a 2.125 MeV gateway, these being ^{183}W ($\sigma\Gamma = 2 \times 10^{-26}$ cm^2-keV) and ^{199}Hg ($\sigma\Gamma = 2 \times 10^{-26}$ cm^2-keV).

Although the contributions of neutron capture processes were included in the analysis above, interferences due to inelastic neutron scattering have not been considered. The cross section σ_{fast} for the $^{176}Lu(n,n')^{176}Lu^m$ reaction was not available in the barn book (BNL 325),[16] probably because of the low natural abundance of ^{176}Lu. However, if the assumption is made that the observed activation was entirely due to inelastic neutron scattering, the cross section required for the scattering process can be calculated from the relation

$$N_{e,fast} = N_T \phi_{fast} \sigma_{fast} t_e \quad , \qquad (10)$$

where ϕ_{fast} is the fast neutron flux. In the previous study of neutron effects,[1] it was estimated that the total fast neutron flux at the sample location was about 900 n/(cm^2-s). Using this estimate, one obtains a value of approximately 2800 barns for σ_{fast}. This is three to four orders of magnitude greater than typical values of cross sections for inelastic neutron scattering, which are normally in the range of several hundred millibarns. On the basis of this result, it appears unlikely that inelastic neutron scattering plays a role in the phenomena examined here.

Conclusions

The large photoactivation cross section obtained for ^{176}Lu in the 1-6 MeV range is consistent with the empirical trend noted for other nuclides in the island of high-mass isomers lying near A = 180. Determination of the nature and location of the gateways responsible for this phenomena will require some form of energy selective x-ray source. As in previous experiments, interferences due to neutron reactions appear to play a minor role in activating the sample.

References

1. J. A. Anderson, C. D. Eberhard, J. J. Carroll, M. J. Byrd, C. B. Collins, E. Scarbrough, and P. P. Antich, "Limits on Neutron Activation Interferences in Photoactivation Cross Section Measurements in the 1.5-6 MeV Range," in Center for Quantum Electronics Report #GRL/8801, University of Texas at Dallas, 1988 (unpublished), pp. 43-72.

2. C. B. Collins, C. D. Eberhard, J. W. Glesener, and J. A. Anderson, Rapid Communications, Phys. Rev. C 37, 2267 (1988).

3. C. B. Collins, J. A. Anderson, C. D. Eberhard, J. F. McCoy, J. J. Carroll, E. C. Scarbrough, and P. P. Antich, "Large Changes of Angular Momenta Pumped by Bremsstrahlung in Selected Nuclei," in Center for Quantum Electronics Report #GRL/8703, University of Texas at Dallas, 1987 (unpublished), pp. 37-56.

4. J. A. Anderson, C. D. Eberhard, J. F. McCoy, K. N. Taylor, J. J. Carroll, M. J. Byrd, C. B. Collins, E. C. Scarbrough, and P. P. Antich, "Photoactivation of Short-Lived Isomers with Bremsstrahlung Radiation from a Medical Linear Accelerator," in Center for Quantum Electronics Report #GRL/8704, University of Texas at Dallas, 1988 (unpublished), pp. 11-35.

5. E. B. Norman, T. Bertram, S. E. Kellogg, S. Gil, and P. Wong, Astrophys. J. 291, 834 (1985).

6. M. A. Gardner, D. G. Gardner, and R. W. Hoff, in Capture Gamma-ray Spectroscopy 1987, Inst. Phys. Conf. Ser. No. 88/J. Phys. G: Nucl. Phys. 14 Suppl., S315 (1987).

7. H. Beer and F. Keppeler, Phys. Rev C 21, 534 (1980).

8. J. J. Carroll. J. A. Anderson, J. W. Glesener, C. D. Eberhard, and C. B. Collins, "Accelerated Decay of $^{180}Ta^{m}$ and ^{176}Lu in Stellar Interiors Through (γ,γ') Reactions," in Center for Quantum Electronics Report #GRL/8803, University of Texas at Dallas, 1989 (unpublished).

9. K. Han, D. Ballon, C. Chui, and R. Mohan, Med. Phys. 14, 414 (1987).

10. R. Mohan, C. Chui, and L. Lidofsky, Med. Phys. 12, 93 (1987).

11. Table of Isotopes, Seventh Edition, Eds. C. M. Lederer and V. S Shirley (Wiley-Interscience, New York, 1978).

12. G. F. Knoll, Radiation Detection and Measurement (John Wiley & Sons, New York, 1979) pg. 746.

13. B. D. Sowerby, Nucl. Instrum. and Meth. 97, 145 (1971).

14. J. K. Tuli, Nuclear Wallet Cards (National Nuclear Data Center, Brookhaven National Laboratory, 1985).

15. F. W. Walker, K. G. Miller, and F. Feiner, Eds., Chart of the Nuclides, Thirteench Edition (General Electric Company, San Jose, California, 1983).

16. D. I. Garber and R. R. Kinsey, Eds., Neutron Cross Sections, Volume II: Curves, National Neutron Cross Section Center, Brookhaven National Laboratory, Publication BNL 325.

ACCELERATED DECAY OF $^{180}Ta^{m}$ AND ^{176}Lu IN STELLAR INTERIORS THROUGH (γ,γ') REACTIONS

by J. J. Carroll, J. A. Anderson, J. W. Glesener, C. D. Eberhard, and C. B. Collins
Center for Quantum Electronics, University of Texas at Dallas

Introduction

The study of naturally occurring radioactive isotopes such as ^{176}Lu and ^{180}Ta has become increasingly important to the astrophysical community since these species have been envisioned as stellar chronometers. Provided the mechanisms of nucleosynthesis are sufficiently understood, the creation of these types of nuclei can be dated from their predicted initial abundance, their presently observed abundance and their half-lives.

The analysis for ^{176}Lu and ^{180}Ta is complicated by the fact that each possesses an isomer. In these cases stellar nucleosynthesis may branch to both the ground state and the isomer, providing a different initial population in each state than would result were only a single level present. This branching is critical to the observation of $^{180}Ta^{m}$, nature's rarest stable isotope,[1] because the isomer ($T_{1/2} \geq 1.2 \times 10^{15}$ years) is the surviving state rather than the shorter lived ground state ($T_{1/2}$ = 8.152 hours).

The presence of an isomer produces an additional effect when the excited nucleus can undergo transmutation without first decaying radiatively to the ground state. If there is a sufficiently strong channel for the transfer of a population of nuclei between the ground state and the isomer, the effective half-lives of the states will be drastically different in the stellar environment than those measured in the laboratory. Processes which may provide such a channel include photoexcitation, positron annihilation excitation, inelastic neutron

scattering and Coulomb excitation. In particular, for ^{176}Lu and ^{180}Ta, photoexcitation through (γ,γ') reactions has been investigated.[2,3]

Critical early works[2,3] described experiments in which samples containing naturally abundant lutetium and tantalum were irradiated with medical ^{137}Cs and ^{60}Co sources. Following exposure, the x-ray spectra of the samples were examined for signatures of the decays of $^{176}Lu^{m}$ and ^{180}Ta. No activation of the tantalum sample was in evidence but some activation of the lutetium sample was observed. In order to calculate the reaction cross section for ^{176}Lu from the observed activation and to estimate an upper bound on the cross section for $^{180}Ta^{m}$, it was assumed that the reactions were non-resonant, threshold processes in keeping with conclusions from previous experiments[4,5] on ^{115}In and ^{111}Cd. The irradiating spectrum was therefore integrated above the assumed threshold and the large number of available photons resulted in the report of small values for the cross sections. The absence of larger cross sections was then used to imply the usefulness of ^{176}Lu and $^{180}Ta^{m}$ nuclei as stellar chronometers.

In contrast to earlier work, the most recent studies of the reactions $^{115}In(\gamma,\gamma')^{115}In^{m}$ and $^{111}Cd(\gamma,\gamma')^{111}Cd^{m}$ have shown no evidence for the appearance of non-resonant effects.[6,7,8,9] Instead it was reported that previous evidence for threshold processes could be attributed to departures of the experimental photon sources from expectations. Evidently (γ,γ') reactions proceed through relatively narrow resonant "gateway" levels rather than through non-resonant excitation. In this context, the most recent measurements[10,11] of the cross sections for the reactions $^{176}Lu(\gamma,\gamma')^{176}Lu^{m}$ and $^{180}Ta^{m}(\gamma,\gamma')^{180}Ta$ make possible a reevaluation of the degree to which these nuclei are useful as stellar chronometers.

Experimental Detail and Analysis

A set of experiments was performed by exposing lutetium and tantalum samples to the bremsstrahlung from a Varian Clinac 1800 medical linear accelerator operating in a 6 MeV mode. An enriched tantalum sample containing 1.3 mg of $^{180}Ta^{m}$ in 24.7 mg of ^{181}Ta was used. The

tantalum was deposited as a dusting of oxide near the center of a 5 cm square plate of aluminum. This sample composition was chosen in order to minimize the self-absorption of fluorescent x- ays. Following irradiation, the sample was transported to an N-type HPGe spectrometer system for counting. As the ground and isomeric states of ^{180}Ta decay by β^- emission and electron capture, as shown by the partial decay level diagram of Fig. 1(a), the 4096-channel pulse-height spectra contained x-ray peaks emitted from the daughter nucleus ^{180}Hf. The identities of the observed photopeaks were verified by their energies and counting rate decays. A typical spectrum for the tantalum sample showing the ^{180}Hf K_α and K_β peaks is given in Fig. 2.

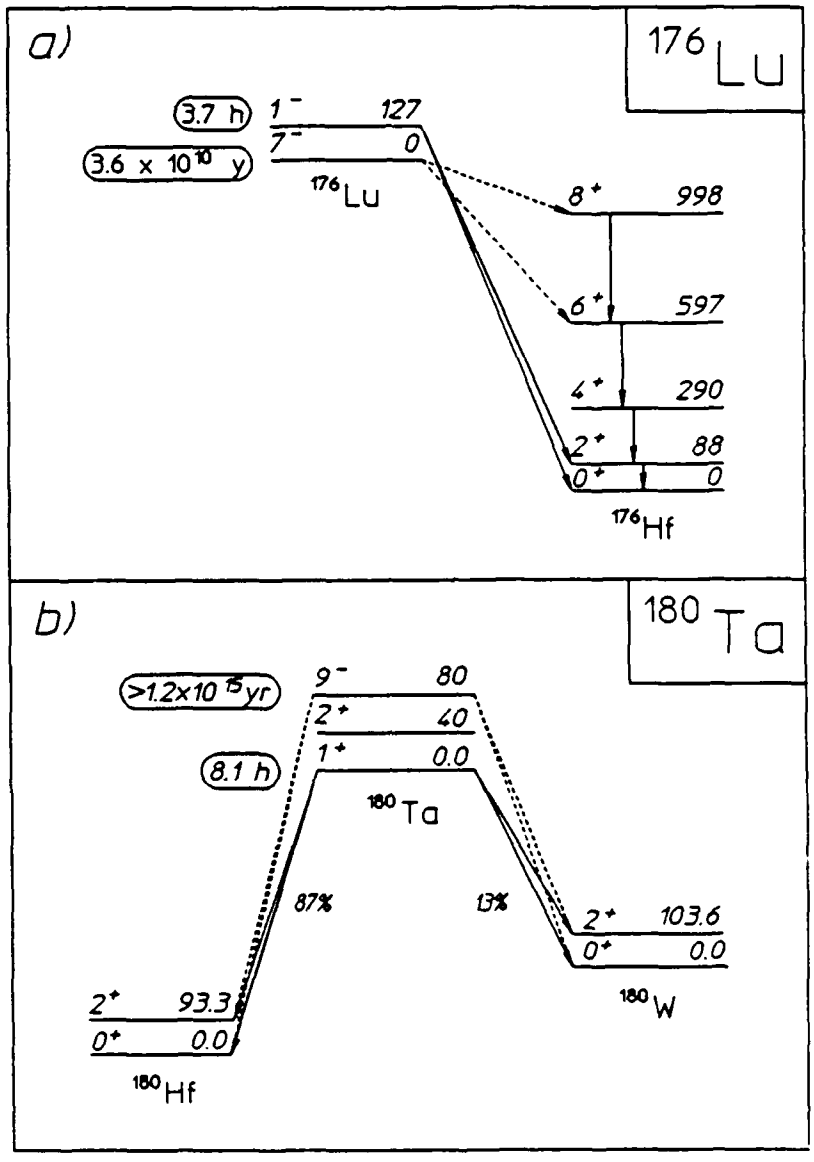

Figure 1: Partial decay level diagrams of a) ^{176}Lu and b) ^{180}Ta depicting parent and daughter nuclei. Half-lives are shown in ovals to the left of the ground and isomeric levels. The nuclear spins, parities, and energies in keV of each state is given. β^- decays are shown by diagonal arrows on the right of the parent levels and electron capture decays are shown by diagonal arrows on the left.

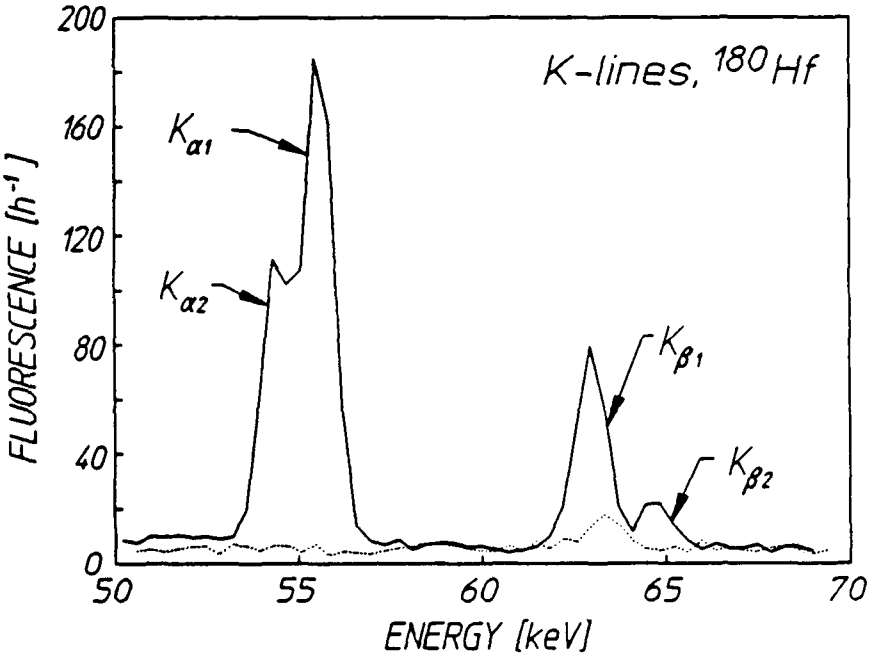

Figure 2: Dotted and solid curves show, respectively, the spectra obtained before and after irradiation of a tantalum sample containing ^{180}Ta enriched to 5%. An HPGe detector was used to obtain the spectra. The feature at 63 keV is due to traces of natural activity in the counting shield. The solid curve shows activity resulting from the transmutation of ^{180}Ta ground state nuclei measured in the sample following irradiation. The prominent additions are the ^{180}Hf K_α and K_β x-ray lines resulting from electron capture in the ^{180}Ta.

Each lutetium sample consisted of approximately 5 g of $LuCl_3$ dissolved in distilled water to make about 20 ml of solution contained within a polyethylene scintillation bottle. The samples were fashioned in this way in order to employ an alternate detection scheme which was better suited to the examination of ^{176}Lu. The ground state of ^{176}Lu β^- decays with an endpoint energy of 565 keV and the isomer with endpoint energies of 1313 keV (39.6%) and 1225 keV (60.4%), as depicted in the partial decay level diagram of Fig. 1(b). Since these nuclei were suspended in solution, the particles emitted in these decays produced Cerenkov radiation in the water with efficiencies dependent on the

differences in the particle energies and the Cerenkov threshold energy at about 250 keV.

In these experiments the efficiency for production of Cerenkov radiation from isomeric decays was over 10 times larger than that from ground state decays. This made possible an accurate measurement of the number of isomeric decays, and thus of isomeric production from the ground state, by counting the Cerenkov events with a detector consisting of two RCA 8850 photomultiplier tubes in EG & G 9201 bases. The tubes were operated in a coincidence mode by connecting the time synchronized outputs through a 150 MHz Phillips 755 logic unit. This insured that only events detected in coincidence by both tubes were counted, improving the signal to noise ratio. Then, the number of coincident counts as a function of time was stored as a 4096 channel MCS spectra with a 40 sec dwell time. A typical spectrum is shown in Fig. 3. The counter was calibrated with a $^{40}KCl_3$ solution of known activity which emitted β^- particles having roughly the same endpoint energy as $^{176}Lu^m$.

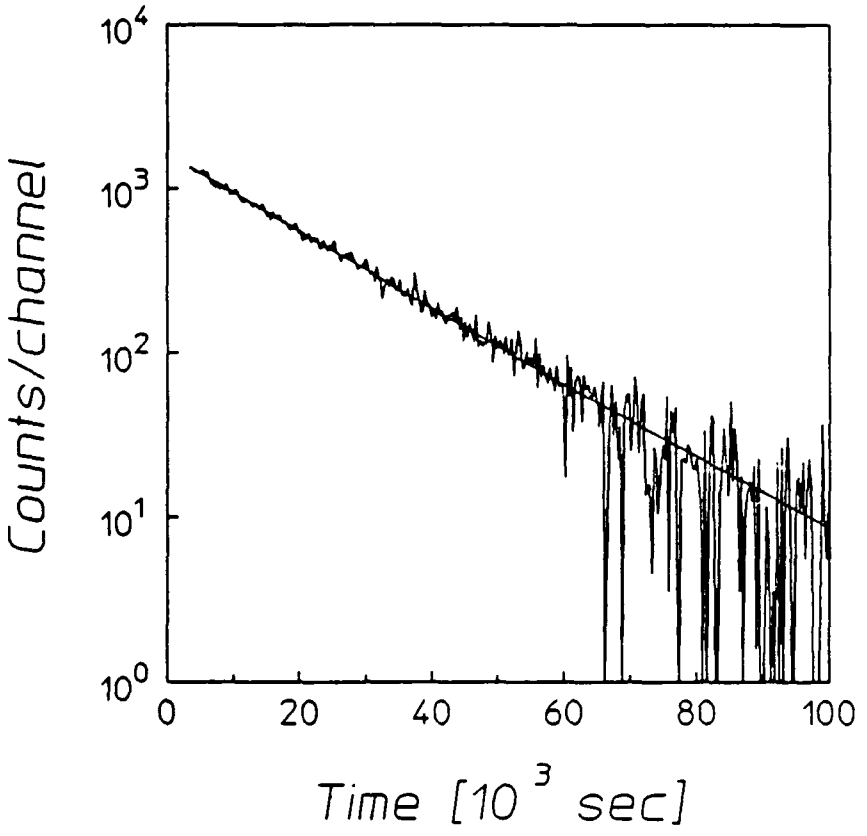

Figure 3: A typical decay spectrum from a lutetium sample following a 40-minute irradiation. Each channel represents an interval of 320 sec. The solid line indicates a fit to the data which gives a half-life for $^{176}Lu^m$ of 3.58 ± .05 h; the literature value is 3.68 hours.

The rate of excitation of nuclei, $dN_{excited}/dt$ was determined for each sample from the observed photopeak counts for the pulse height spectra and from the decay of the counting rate for the coincidence spectra. These were corrected for self-absorption of fluorescent photons, detector efficiency, signature photon or β^- decay intensity and finite times for counting, transport and irradiation. From the viewpoint of photoexcitation through resonant gateways, the excitation rate is given by

$$\frac{dN_{excited}}{dt} = N_T \sum_i (\sigma\Gamma)_i \, \Phi(E_i) \quad , \qquad (1)$$

where N_T is the number of target nuclei in the sample, $\Phi(E_i)$ is the incident photon flux in photons/cm^2-keV-sec at the gateway energy E_i, and $(\sigma\Gamma)_i$ is the integrated cross section in cm^2-keV,

$$(\sigma\Gamma)_i = \int \sigma_i(E)\, dE \quad . \tag{2}$$

The quantity Γ_i represents the natural width of the i^{th} gateway state, given by $\Gamma_i \geq \hbar/\tau_i$ where τ_i is the lifetime of the state. Determinations of the integrated cross sections depend primarily on knowledge of the E_i since the output of the linac is well characterized.[12,13] The relative spectral intensity normalized to unit total flux for the linac operating in the 6 MeV mode is shown in Fig. 4.

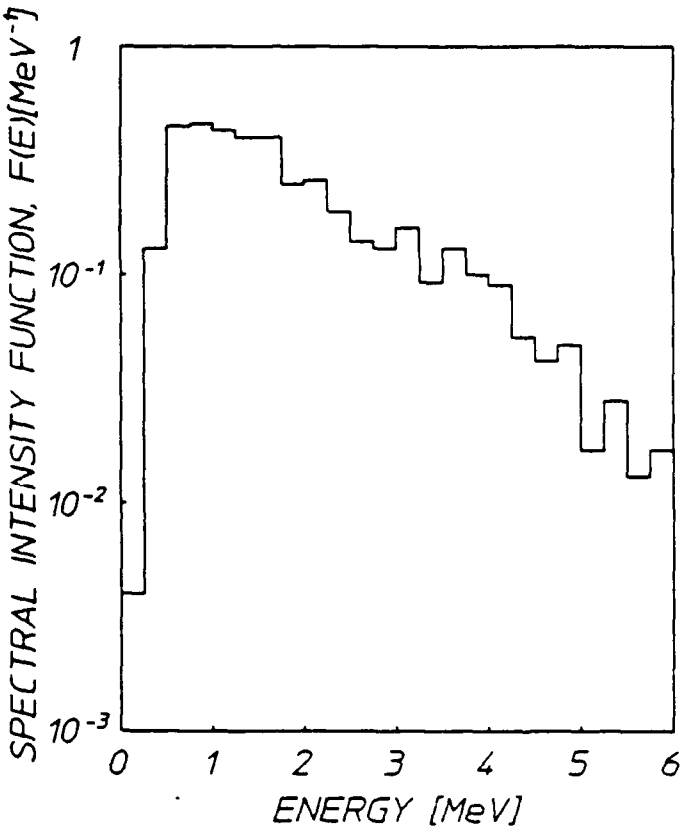

Figure 4: Relative spectral intensities of the bremsstrahlung from the Varian Clinac 1800 used in these experiments. The function F[MeV^{-1}] is normalized to the total delivered flux, which for linac operation in the 6 MeV mode at 300 Hz is 2.28 × 10^7 photons/cm^2-keV-sec at a distance of 63.7 cm from the x-ray source.

The fixed endpoint of the linac did not allow the gateways to be located. However, by assuming the excitation proceeds through a single gateway state, cross sections were found as functions of the possible gateway energies. Previous examinations[14,15,16] of known nuclear states have indicated that the lowest likely gateway states lie at about 1 MeV for ^{176}Lu and about 750 keV for ^{180}Ta^m. Consistent with these suggestions, the cross sections for ^{176}Lu and ^{180}Ta^m are shown in Figure 5. The gateway energies indicated by the data points are located at the centers

of energy bins corresponding to mesh points at which intensities are available from published linac spectra.

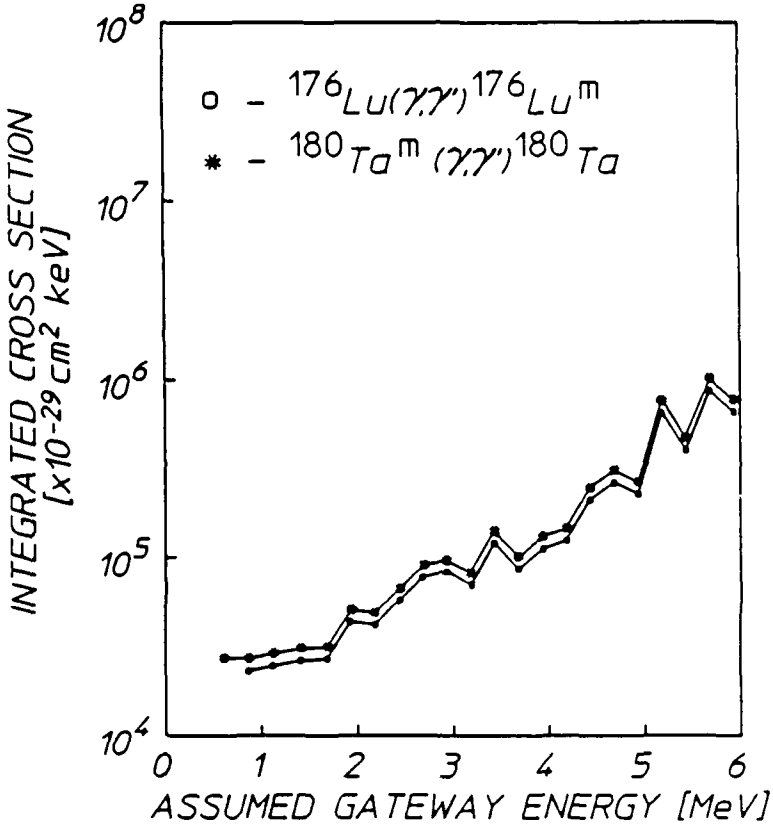

Figure 5: Integrated cross sections for the reactions $^{176}Lu(\gamma,\gamma')^{176}Lu^{m}$ and $^{180}Ta^{m}(\gamma,\gamma')^{180}Ta$, each plotted as a function of the energies at which a single gateway state could be assumed.

It is difficult to directly compare the results of Fig. 5 with the cross sections of Refs. 2 and 3 since the irradiating spectra used in those experiments are not known. However, as a point of contact between the two approaches, for $^{180}Ta^{m}$ a single resonant gateway at 750 keV would correspond to an integrated cross section of 27700 $\times$ 10^{-29} cm^2-keV while a non-resonant process with a threshold at 750 keV would have a cross section of 148 μbarns. This is more than 3 orders of magnitude larger than the cross section reported in Ref. 3.

Effective Half-Life of ^{176}Lu

The ground and isomeric states of ^{176}Lu can be considered to comprise two components of a coupled system of populations governed by the standard rate equations for radioactive decay. For the ground and metastable populations N_0 and N_1, these are

$$\frac{dN_1}{dt} = -(R_1 + R_{10})N_1 + R_{01}N_0 \quad , \tag{3}$$

and

$$\frac{dN_0}{dt} = -(R_0 + R_{01})N_0 + R_{10}N_1 \quad . \tag{4}$$

The quantities R_0 and R_1 are the radioactive decay rates for these states, taken from laboratory values for the half-lives, $(T_{1/2})_0 \geq 3.59 \times 10^{10}$ years and $(T_{1/2})_1 = 3.635$ hours. The R_{01} and R_{10} are the total transfer probability rates from ground to isomer and from isomer to ground states through (γ,γ') reactions.

The rate for excitation to the isomer through a single gateway is found by recognizing that $R_{01} = N_T^{-1} \cdot dN_{excited}/dt$, where N_T is the number of target nuclei. Eq. (1) then gives

$$R_{01} = (\sigma_{01}\Gamma)\, \Phi(E_{01}) \quad , \tag{5}$$

where E_{01} is the gateway energy relative to the ground state and the width of the gateway has been assumed to be sufficiently narrow so that the flux may be considered as constant over the gateway. Employing the Plank distribution to represent the stellar interior at temperature T,

$$\Phi(E_{01}) = \frac{8\pi E_{01}^2}{h^3c^2} \left[\exp(E_{01}/kT) + 1\right]^{-1} \quad . \tag{6}$$

Thus, in terms of the experimentally measured integrated cross section,

$$R_{01} = \frac{8\pi}{h^3c^2} (\sigma_{01}\Gamma)\, E_{01}^2 \left[\exp(E_{01}/kT) + 1\right]^{-1} \quad . \tag{7}$$

The rate for the inverse reaction is found by considering the question of thermal equilibrium. If it were possible for both states to come into equilibrium with the photon bath, the net photoexcitation rate would vanish,

$$\left(\frac{dN_1}{dt} + R_1 N_1\right)_{eq.} = 0 \quad . \tag{8}$$

This indicates that as a function of the ground and isomeric state angular momenta J_0 and J_1 and the energy of the isomer relative to the ground state, E_1, the ratio of populations would become,

$$\left(\frac{N_1}{N_0}\right)_{eq.} = \frac{R_{01}}{R_{10}} = \frac{2J_1 + 1}{2J_0 + 1} \exp(-E_1/kT) \quad . \tag{9}$$

For the ^{176}Lu isotope, $J_0 = 7$, $J_1 = 1$ and the isomer energy is $E_1 = 126$ keV. Then, the solution to the rate Eqs. (2) and (3) is given by,

$$\frac{N_1}{N_0}(t) = \frac{a + b \coth(bt/2)}{2R_{10}} \quad , \tag{10}$$

where

$$a = R_0 + R_{01} - R_1 - R_{10} \quad ,$$

and

$$b = \sqrt{a^2 + 4R_{01}R_{10}} \quad .$$

The effective half-life of ^{176}Lu nuclei in the stellar environment is finally evaluated for this two level system from the expression,

$$(T_{1/2})_{eff} = \left[1 + \frac{N_0}{N_1}\left((T_{1/2})_1\right)\right](T_{1/2})_1 \quad . \tag{11}$$

Figure 6 shows the effective half-life as a function of temperature for several assumed gateway energies.

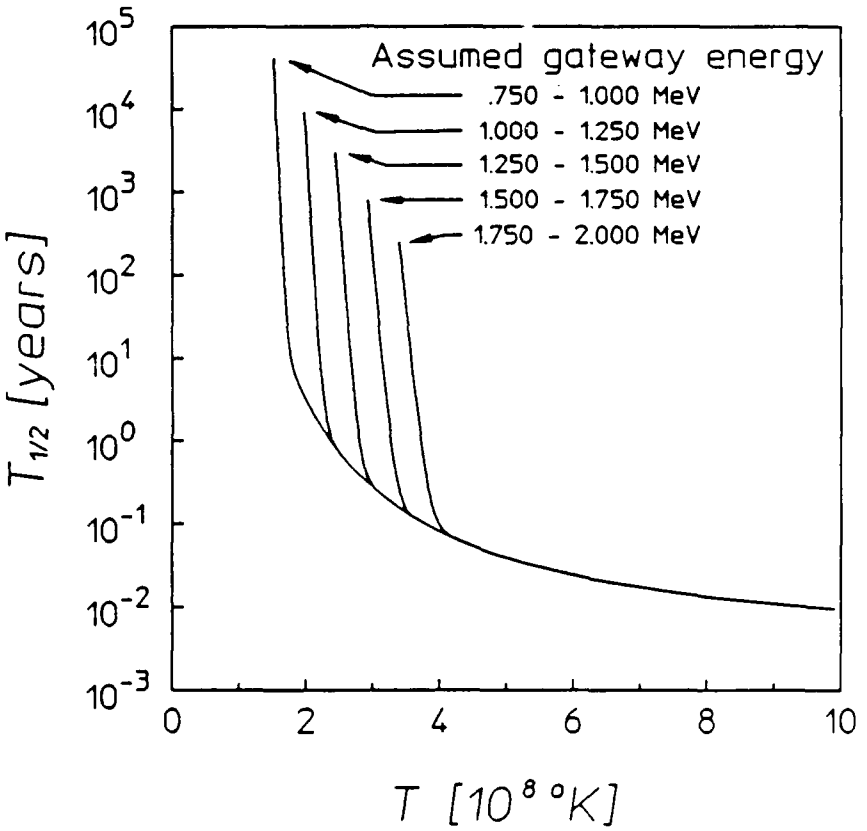

Figure 6: Effective half-life of ^{176}Lu nuclei as a function of the temperature of the stellar environment in which it is immersed. The different curves are parametrized by assumed gateway energies lying in the indicated energy ranges.

Effective Half-Life of ^{180}Ta

The possibility of decay of ^{180}Ta nuclei by electron capture introduces an additional temperature dependence. The half-life of the isomer is so long that an accurate result can be obtained by considering it to be temperature independent. However, the depletion of its electron shells at stellar temperatures will appreciably alter the half-life of the ground state. Detailed calculations of this effect have been made,[17] but the nuclear data that were used are now dated. Considering

the simpler problem of the depletion of the K shell only, the ground state half-life may be written as[18]

$$(T_{1/2})_0 = [(T_{1/2})_0]_{lab.} \; [b_{ec}\, r(T) + b_\beta]^{-1} \quad , \tag{12}$$

where $b_{ec} = .87$ and $b_\beta = .13$ are the branching ratios for the two decay modes. The ratio r(T) of K shell occupancy at T to that as T -> 0 is given by

$$r(T) = [\exp(\mu - E_K/kT) + 1]^{-1} \quad , \tag{13}$$

where $E_K = 67.416$ keV is the K shell energy and μ is the fermion chemical potential,

$$e^\mu = \frac{2}{h^3 N_e} (2\pi m_e kT)^{3/2} \quad , \tag{14}$$

where N_e is the number density of electrons in pure He stellar matter, for which a typical value of 10^3 g/cm^3 is taken and m_e is the electron mass. The half-life of the ^{180}Ta ground state as a function of temperature is given in Figure 7.

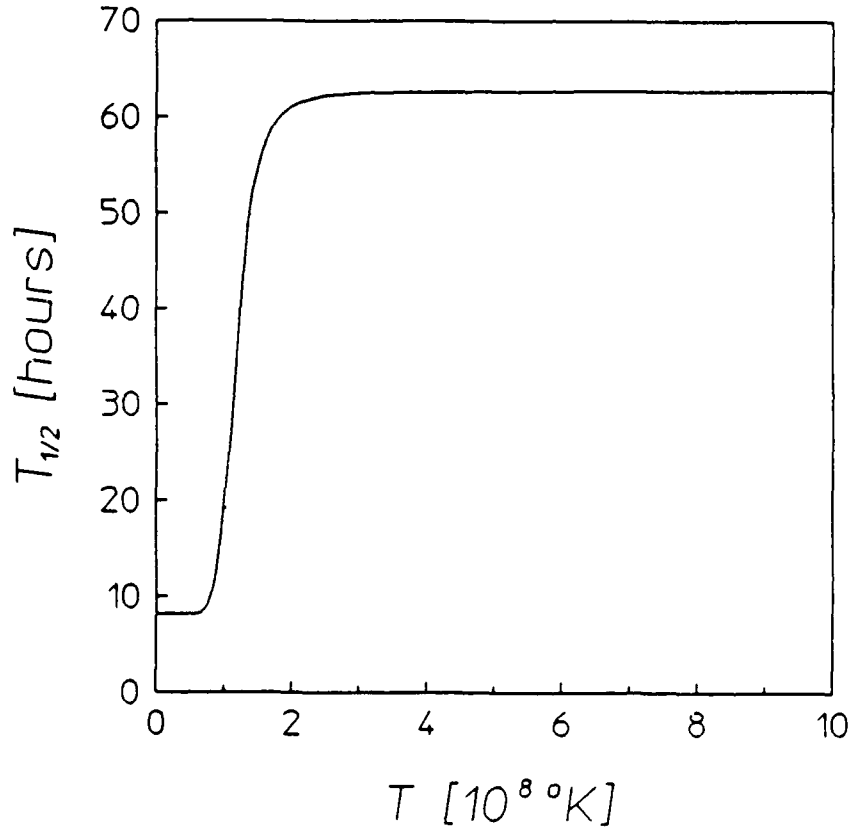

Figure 7: Half-life of ground state nuclei of ^{180}Ta as a function of temperature in the surrounding stellar environment. At temperatures above 2×10^8 °K, the K shell is completely depleted and the nuclei decay only through β^- emission.

With the inclusion of this mechanism, the previous analysis is used to determine the half-life of ^{180}Ta for which $J_0 = 7$, $J_1 = 1$ and $E_1 = 127$ keV from

$$(T_{1/2})_{eff} = \left[1 + \frac{N_1}{N_0} \{(T_{1/2})_0\} \right] (T_{1/2})_0 \quad . \qquad (15)$$

These results are displayed in Figure 8.

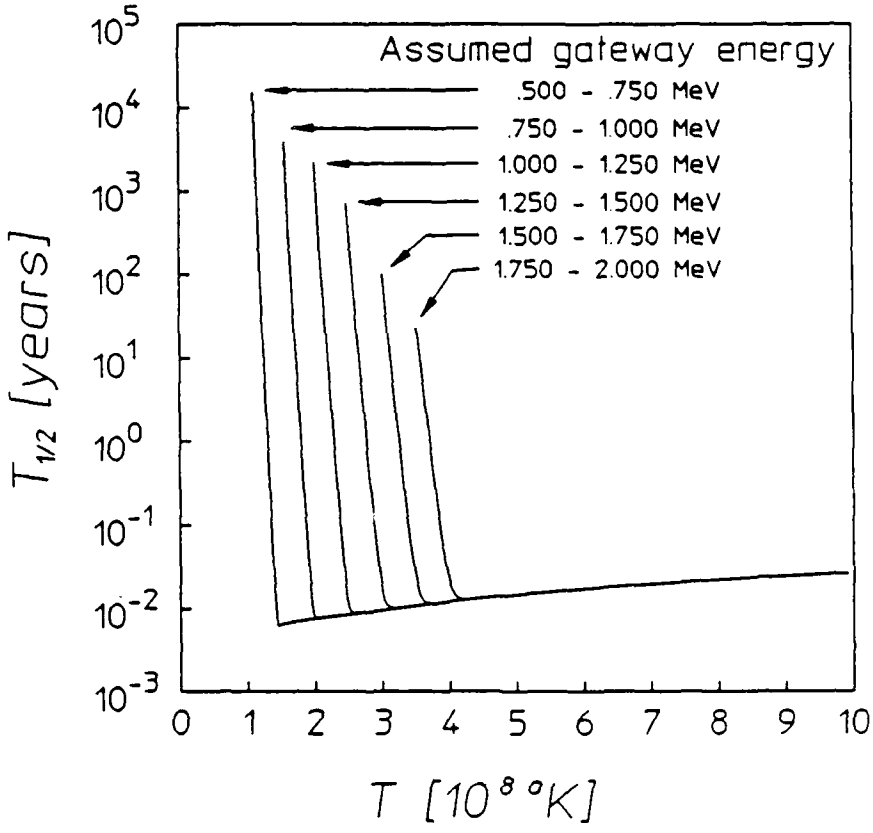

Figure 8: Effective half-life of ^{180}Ta nuclei as a function of the temperature of the stellar environment in which it is immersed. The different curves are parametrized by assumed gateway energies lying in the indicated energy ranges.

Discussion

An origin which is strictly s-process in character has been proposed[19,20] for ^{176}Lu and the appropriate neutron capture chain has been examined.[21,22] This isotope is shielded from the r-process by ^{176}Yb, which is stable against β^- decay. The s-process of stellar nucleosynthesis is thought to require temperatures of around 3.5×10^8 °K and to occur primarily in stable red giants,[23] possibly during thermal relaxation oscillations.[24] Examination of Fig. 6 indicates that at this temperature at least partial equilibration of the ground state and isomer of ^{176}Lu will occur unless the gateway is located at an energy

above about 1.5 MeV. Should the gateway lie within the 1 - 1.25 MeV range as has been suggested, an s-process origin may still apply. However, the strong temperature dependence of the half-life would render ^{176}Lu useless as an s-process chronometer.

Many mechanisms have been suggested to be responsible for the production of ^{180}Ta though none have been firmly established.[25,26] Recently an s-process origin for ^{180}Ta has been suggested[27,28] and the necessary reactions demonstrated.[29] The rarity of $^{180}Ta^{m}$ was concluded to be a consequence of the fact that this nucleus lies aside the main path of cosmic nucleosynthesis.[30] Fig. 8 clearly shows again that equilibrium will occur at the canonical s-process temperature of 3.5×10^{8} °K unless the gateway lies above 1.5 MeV. The discovery of a gateway laying below 1.5 MeV would then imply that ^{180}Ta could not be employed as an s-process chronometer. This could only be avoided if the s-process can proceed at temperatures below 1.5×10^{8} °K.

These interesting results point to the importance of locating the participating gateways more precisely. This could be accomplished if a variable endpoint linac were available that was capable of delivering sufficient dosage. Indeed, should multiple gateways be found below 6 MeV the results of this analysis may be drastically altered. Also of importance is the more manageable problem of determining the linac spectrum for smaller bin sizes. Each curve in Figs. 6 and 8 must represent a range in possible gateway locations rather than simply one gateway energy. Smaller bin sizes would enable more exact examination of the temperatures at which equilibration becomes important for given gateway locations.

References

1. A. G. W. Cameron, Essays in Nuclear Astrophysics, edited by C. A. Barnes, D. D. Clayton, and D. N. Schramm (Cambridge Univ. Press, Cambridge, 1982), p. 23.
2. E. B. Norman, T. Bertram, S. E. Kellogg, S. Gil, and P. Wong, Ap. J. 291, 834 (1985).
3. E. B. Norman, S. E. Kellogg, T. Bertram, S. Gil, and P. Wong, Ap. J. 281, 360 (1984).
4. A. Ljubicic, K. Pisk, and B. A. Logan, Phys. Rev. C 23, 2238 (1982).
5. M. Krcmar, A. Ljubicic, K. Pisk, B. Logan, and M. Vrtar, Phys. Rev C 25, 2097 (1981).
6. K. Yoshihara, Zs. Nemeth, L. Lakosi, I. Pavlicsek, and A. Veres, Phys. Rev. C 33, 728 (1986).
7. I. Bikit, J. Slivka, I. V. Anicin, L. Marinkov, A. Rudic, and W. D. Hamilton, Phys. Rev. C 35, 1943 (1987).
8. C. B. Collins, J. A. Anderson, Y. Paiss, C. D. Eberhard, R. J. Peterson, and W. L. Hodge, Phys. Rev. C 38, 1852 (1988).
9. J. A. Anderson, M. J. Byrd, and C. B. Collins, Phys. Rev. C 38, 2838 (1988).
10. J. A. Anderson, K. N. Taylor, J. J. Carroll, M. J. Byrd, C. B. Collins, E. C. Scarbrough, and P. P. Antich, Center for Quantum Electronics Report #GRL/8803, University of Texas at Dallas, 1988 (unpublished).
11. C. B. Collins, C. D. Eberhard, J. W. Glesener, and J. A. Anderson, Phys. Rev. C 37, 2267 (1988).
12. R. Mohan, C. Chui and L. Lidofsky, Med. Phys. 12, 595 (1985).

13. N. C. Ikoro, D. A. Johnson, and P. P. Antich, Med. Phys. 14, 93 (1987).

14. R. A. Dewberry, R. K. Sheline, R. G. Lanier, L. G. Mann, and G. L. Struble, Phys. Rev. C 24, 1628 (1981).

15. O. A. Wasson and R. E. Chrien, Phys. Rev. C 2, 675 (1970).

16. E. Warde, R. Seltz, G. J. Costa, D. Magnac, and C. Gerardin, Phys. Rev. C 27, 98 (1983).

17. K. Takahashi and K. Yokoi, At. Data and Nuc. Data Tables 36, 375 (1987).

18. B. Stromgren, Zeits. fur Ap. 4, 118 (1932).

19. J. Audouze, W. A. Fowler, and D. N. Schramm, Nature 238, 8 (1972).

20. M. Arnould, Astr. Ap. 22, 311 (1973).

21. B. J. Allen, G. C. Lowenthal, and J. R. de Laeter, J. Phys. G 7, 1271 (1981).

22. H. Beer, F. Kappeler, K. Wisshak, and R. A. Ward, Ap. J. Suppl. 46, 295 (1981).

23. An Introduction to Nuclear Astrophysics, J. Audouze and S. Vauclair (D. Reidel Publishing Company, Boston, 1979).

24. Astrophysics, W. K. Rose (Holt, Rinehart, and Winston, Inc., New York 1973).

25. J. Audouze, Ast. Ap. 8, 436 (1970).

26. K. L. Hainebach, D. N. Schramm, and J. B. Blake, Ap. J. 205, 920 (1976).

27. H. Beer and R. A. Ward, Nature 291, 308 (1981).

28. K. Yokoi and K. Takahashi, Nature 305, 198 (1983).

29. S. E. Kellogg and E. B. Norman, Phys. Rev. C 31, 1505 (1985).

30. E. Runte, W. D. Schmidt-Ott, W. Eschner, I. Rosner, R. Kirchner, O. Klepper, and K. Rykaczewski, Z. Phys. A 328, 119 (1987).

N00014-86-C-2488
UTD #24522-964

SPECTRAL CHARACTERIZATION OF INTENSE, SHORT DURATION BREMSSTRAHLUNG PULSES WITH NUCLEAR PHOTOACTIVATION TECHNIQUES

by J. A. Anderson, C. D. Eberhard, K. N. Taylor, J. M. Carroll, J. J. Carroll, M. J. Byrd, and C. B. Collins
Center for Quantum Electronics, University of Texas at Dallas

Introduction

Pulsed power machines that generate high intensity x-ray pulses are often used to assess the radiation hardness of electronic components and systems but have also recently found application in research programs studying ultrashort wavelength (gamma-ray or x-ray) laser mechanisms. For this research, an accurate understanding of the bremsstrahlung spectrum emitted by the machine is necessary. This information can also be of interest to the nuclear simulation community if radiation hardness tests are required to mimic the average photon energy as well as the total dose and dose rate for the simulated operating environment. Unfortunately, the x-ray spectrum of such a device is difficult to determine and in practice is often estimated using Monte Carlo transport calculations in lieu of being experimentally measured. This paper discusses the use of resonant photonuclear activation as a simple experimental technique that can be used on a shot-by-shot basis to characterize these spectra.

A pulsed power bremsstrahlung generator can readily deliver doses of several tens of kRads in an x-ray pulse lasting less than 100 ns. Endpoint energies for the bremsstrahlung can range from near 1 MeV up to about 10 MeV. Because of the magnitude of energy expended in each pulse, practical devices built to deliver these doses can only fire a few times each day. This combination of high flux, high photon energy, and very low duty cycle presents a problem for conventional measurement techniques.[1] Energy dispersive methods using scintillators or solid state detectors are statistically limited by the small number of events that can be pulse height analyzed during an x-ray burst that lasts less than 100 ns and which can be repeated only after several hours. Standard techniques for wavelength dispersive x-ray spectroscopy with crystal spectrometers are practical only in the region below about 150

keV due to the range of available lattice spacings. Thus, neither of the two most commonly used tools for x-ray spectroscopy is well suited for characterizing these radiation pulses.

The sensitivity of absorption spectrometers,[2] which obtain a spectrum by deconvolving the responses of arrays of differently filtered dosimeters, is limited to the range where mass attenuation coefficients vary strongly with energy. This is well below 1 MeV. A second technique, that of photoneutron spectroscopy, suffers from the converse problem of being insensitive at low energies. At photon energies high enough to induce (γ,n) reactions, the resulting photoneutrons can be detected with activation foils, and this information can be used to deconvolve the incident x-ray flux. Unfortunately, there are only two materials with photoneutron thresholds E_n below 3 MeV, these being ^2H (E_n = 2.22 MeV) and ^9Be (E_n = 1.67 MeV); even if the energy range is extended to 6 MeV, only 8 isotopes are suitable for this application.[3] The photoneutron technique requires high photon fluxes and may also suffer from interferences in mixed radiation fields.

Another approach to characterizing bremsstrahlung pulses is to analyze the momentum of Compton scattered electrons emitted from a material illuminated by the x-ray pulse and from this information to deduce the spectrum of the incident radiation.[4] This approach is theoretically capable of dealing with a wide energy range, but it is complex and costly to implement.

The limitations of the techniques outlined above are graphically summarized in Fig. 1. Resonant nuclear photoactivation is a method which complements these techniques and which requires little in the way of specialized equipment. It may be the only practical approach in some applications.

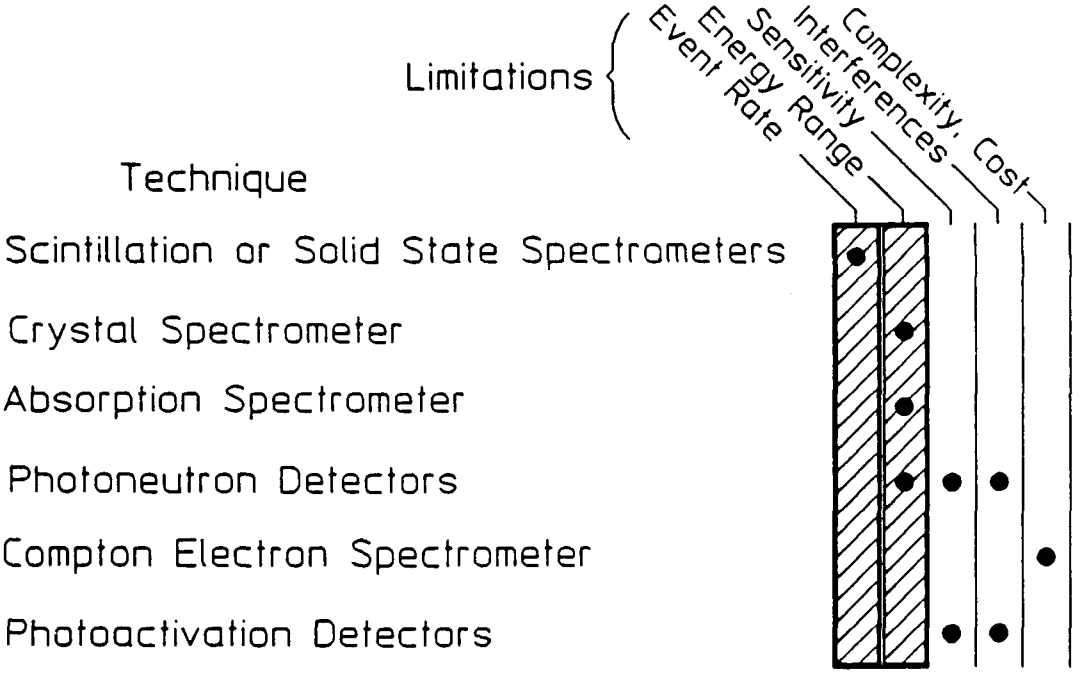

Figure 1: Limitations of different measurement techniques for measuring short (< 100 ns), non-repetitive x-ray bursts. The shaded area includes major limitations that may exclude, in general, the use of a given method.

Resonant Nuclear Photoactivation Detectors

Determining photon fluxes with resonant nuclear photoactivation of nuclear isomers is analogous to monitoring fast neutron fields with neutron activation foils, with one important difference: neutron activation foils are threshold detectors, but photoactivation monitors determine the photon flux in a narrow window at the resonance energy. The process is illustrated in Fig. 2. Incident photons excite the ground state to a short-lived intermediate, or gateway, state that promptly decays to form an isomer. The exposed sample can then be transported to a conventional counting system and the population of the isomeric state can be quantified. From this information and the value of the transfer cross section, the photon flux at the gateway energy can be obtained. If several materials with different gateway energies are available, the spectrum of the incident radiation can be deduced as shown in Fig. 3.

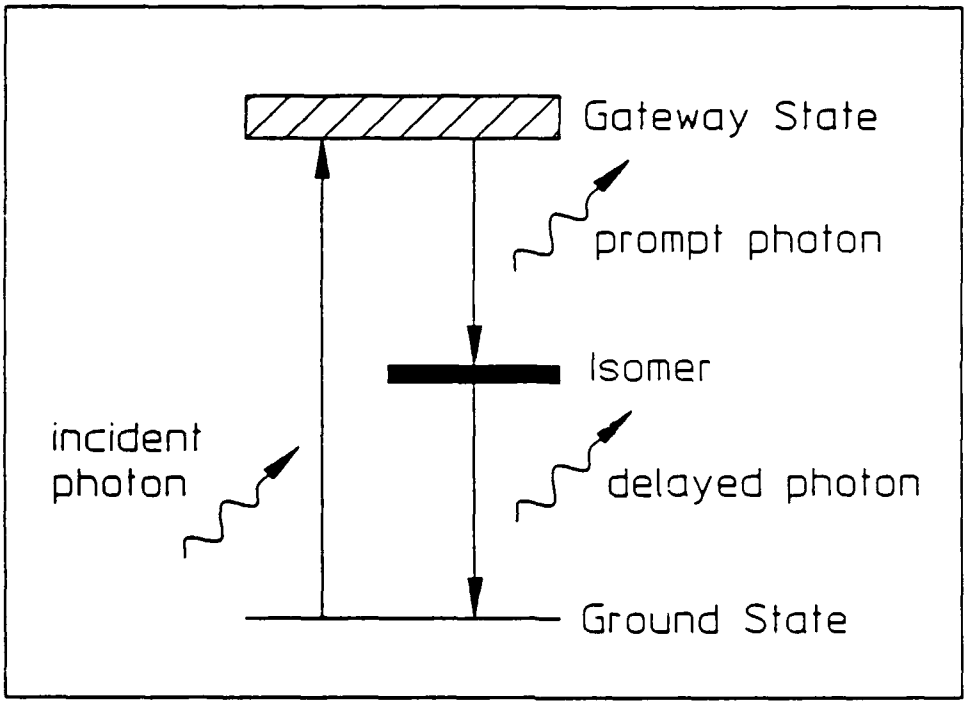

Figure 2: Mechanism of resonant photo-activation of nuclear isomeric states. Given the transfer cross section through the gate-way state, the number of delayed photons emitted can be used to determine the incident photon flux.

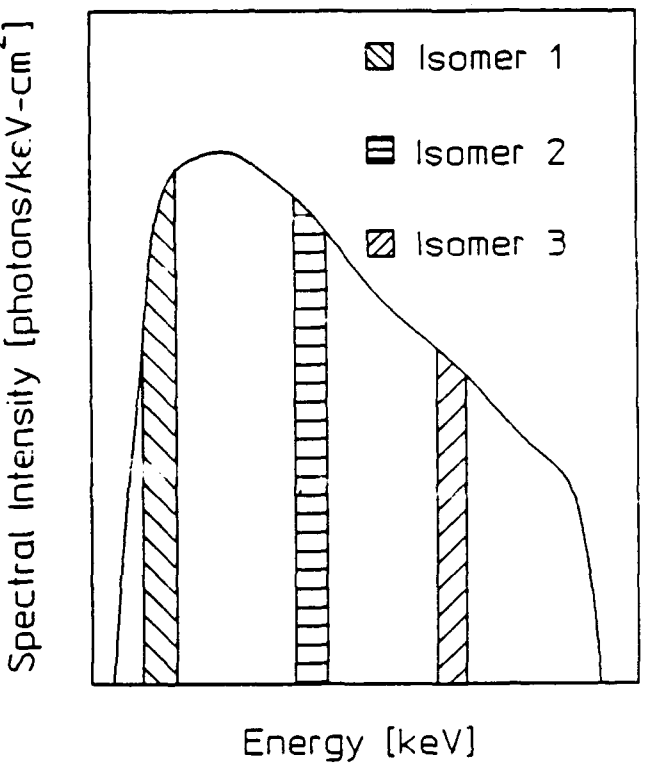

Figure 3: The technique for determining an x-ray spectrum using nuclear photoactivation. Isomers having different gateway states provide measurements of the spectral intensity in specific energy windows.

One complication of this scheme is that isomeric materials in general will possess more than one gateway, thus necessitating a more complicated deconvolution than the idealized case given above. If the irradiation pulse is short compared to the half-lives of the isomeric states involved, the isomeric population can be written as

$$N_{excited} = N_o \sum_i [\pi b_a b_o \sigma_o \Gamma/2]_i \ \phi(E_i) \quad , \qquad (1)$$

where N_o is the number of target nuclei in the sample, the quantity in brackets is the effective integrated cross section for transfer through the ith gateway state, $\phi(E_i)$ is the incident photon flux at the energy E_i of the ith gateway, and the summation is taken over all accessible gateways. The terms appearing in the integrated cross section are the Breit-Wigner cross section, σ_o, the width of the resonance, Γ, and the branching ratios from the gateway state to the ground and excited

states, b_a and b_o. The units of the integrated transfer cross section are cm^2-keV; the units for the photon flux are photons/cm^2-keV.

One of the major difficulties in implementing resonant photoactivation detectors is obtaining good values for the energy and cross section parameters of the gateway states. A summary of parameters appropriate for measurements in the range below 1.5 MeV is given in Table I.[5,6,7]

Table I: Resonant photoactivation parameters for measurements below 1.5 MeV. The integrated cross section corresponds to the term appearing in brackets in Eq. (1). Branching ratios for the decay are not given but may be found in the literature.[8]

Isomer	Isomeric Energy [keV]	Gateway Energy [keV]	Cross Section [10-29 cm^2-keV]	Observed Decay Energy [keV]	Half-life
$^{79}Br^m$	207	761	6.2	207	4.86 s
$^{77}Se^m$	162	250	0.2	162	17.4 s
			480*	0.87	
			818	0.7	
			1005	30.	
$^{115}In^m$	336	1078	18.7	336	4.486 h
$^{111}Cd^m$	396	1190	9.8	245	48.6 m

*This represents the weighted average of two levels at 440- and 521-keV.

The experimental arrangement for this type of work is illustrated in Fig. 4. Samples may be mounted either in a stationary fixture or inside a pneumatic transfer system. After the exposure, they are transported to a conventional spectroscopy system in a remote area for counting. The equipment can be made readily portable and requires only limited space in the test cell. In normal operation, the x-ray device will automatically trigger the transfer system and a transit timer. Arrival of the sample at the detector stops this timer and starts the spectrometer acquisition cycle. The resulting spectra are analyzed for photopeak areas, from which the total number of excited states produced by the irradiation can be calculated.

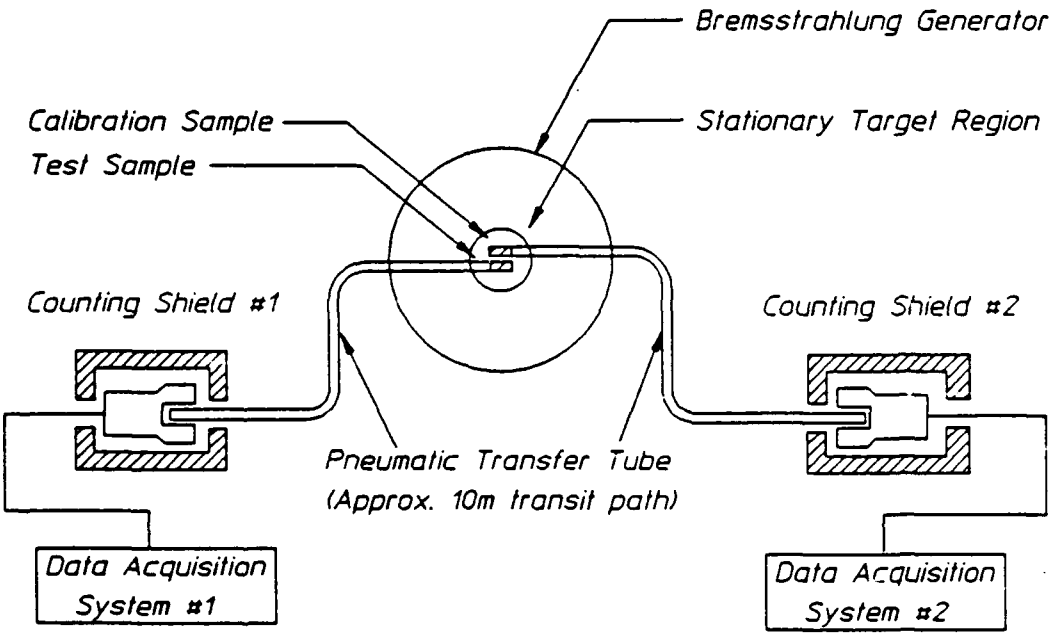

Figure 4: Apparatus for the implementation of nuclear photoactivation measurements.

Example: Bremmstrahlung Endpoint < 1.5 MeV

The cross sections shown in Table I were obtained in a series of experiments[5,6,7] conducted with the DNA/PITHON flash x-ray device, operated by Physics International in San Leandro, CA. In this work, the endpoint of the machine was varied from about 1.0 to 1.5 MeV, and the dose delivered to the samples ranged up to approximately 20 kRad. An example of the type of data obtained with a single shot of PITHON is shown in Fig. 5. By using TIGER[9] code calculations for the variation of the spectral intensity as a function of endpoint energy, it was possible to standardize all of the gateway parameters listed in Table I against the values for ^{79}Br, which were considered to be the best information from the literature. A comparison of the experimental results for a particular shot and the TIGER code calculation for the same shot, adjusted for the estimated source-sample separation, is shown in Fig. 6.

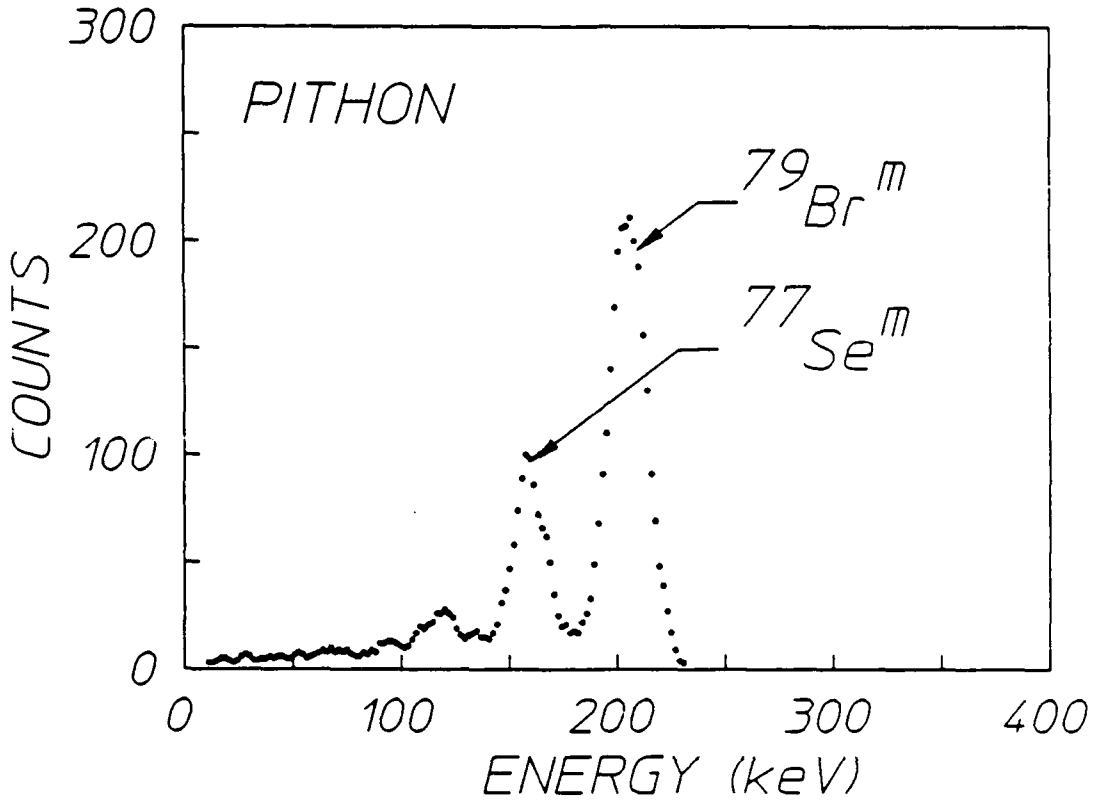

Figure 5: NaI(Tl) spectrum obtained following a single irradiation at the PITHON x-ray facility. The sample was a mixture of 1.25 g of LiBr and 1.20 g of Se powder. Acquisition time was 80 s.

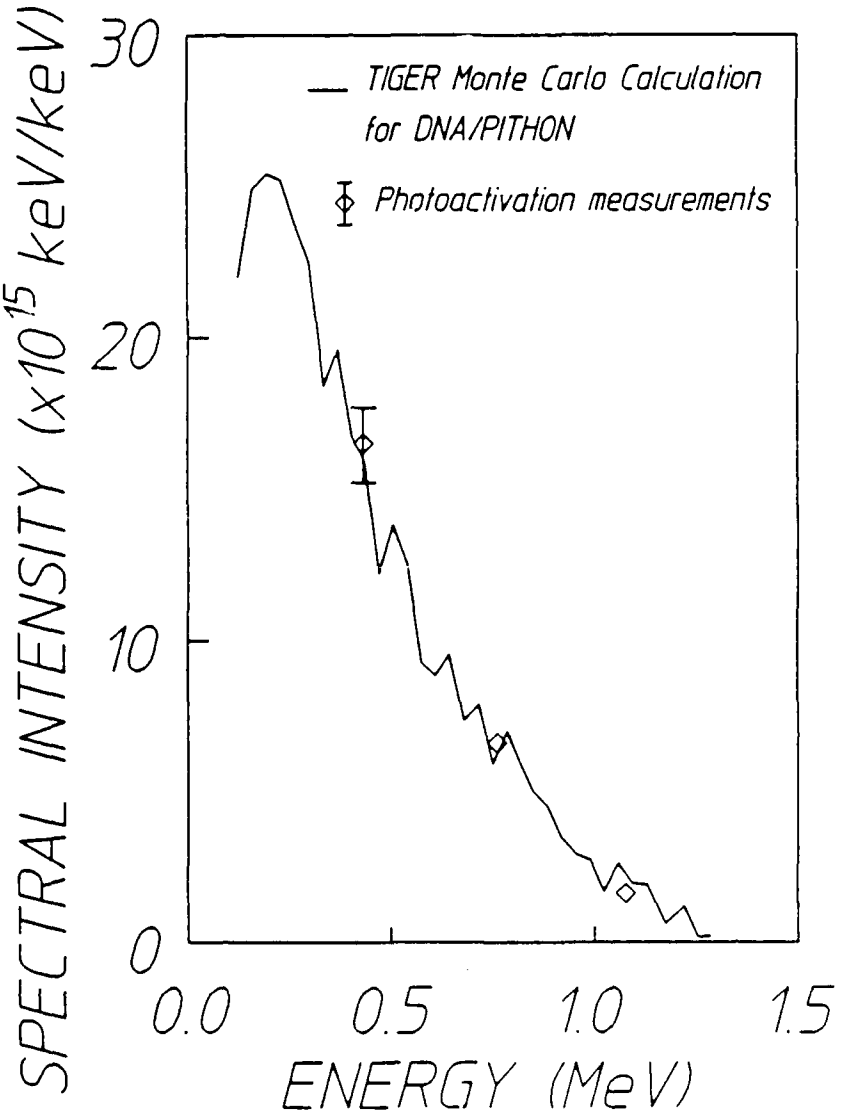

Figure 6: Comparison of calculated (solid line) and measured (diamonds) spectral intensity for PITHON shot 4379.

Example: Bremmstrahlung Endpoint > 1.5 MeV

As the endpoint energy of the x-ray spectrum is increased, more reaction channels open. This complicates the situation by allowing interfering reactions to compete with the selected photoactivation process. These competing channels may be (γ,n) reactions, (n,γ) reactions with the neutrons produced in the environment by high energy source photons, and additional (γ,γ') reactions with high gateway energies.

In experiments conducted at the U.S. Army's Harry Diamond Laboratory in Adelphi, MD, bremsstrahlung from the Aurora machine with a nominal endpoint of 10 MeV was used to further study the use of photoactivation as a spectral characterization tool. This device, which develops 14 TW of electrical power, is the world's largest flash x-ray machine. In one mode of operation, the direct output of the machine is softened by Compton backscattering in a large block of plastic in an arrangement similar to that described in Ref. 2. In this case, the test volume is in a massive high Z shield that prevents the unscattered radiation from illuminating the devices or samples under study. Because the Compton scattering is occurring at close to 180°, the peak in the softened spectrum is expected to lie near 100 keV. Measurements with an absorption spectrometer confirm this.[10]

A set of photoactivation measurements were made in this softened environment and were analyzed in the manner described above. However, significant differences were encountered in this data. An example of the data obtained in this work is shown in Fig. 7. It was not possible to observe photoactivation in the indium sample in this case because of strong interference from the $^{115}In(n,\gamma)^{116}In^{m}$ reaction, which has large cross sections in the thermal and resonance regimes. High energy source photons interacting in the plastic block through $^{2}H(\gamma,n)^{1}H$ reactions created the slow neutrons responsible for the interference. By counting both bare and cadmium covered foils, it was possible to quantify ϕ_{th}' and ϕ_{epi}', the thermal and epithermal neutron fluxes in the sample region, normalized to the delivered dose. The values $\phi_{th}' = (4.2 \pm 0.3) \times 10^{6}$ n/(cm^2-kRad) and $\phi_{epi} = (9.5 \pm 0.6) \times 10^{4}$ n/(cm^2-kRad) were obtained using conventional analysis techniques.[11,12] From these values, it was possible to calculate the degree of neutron contamination in the ^{77}Se and ^{111}Cd measurements. The ^{77}Se observation shown in Fig. 7 was found to be dominated by neutron capture interferences, but only about 15% of the $^{111}Cd^{m}$ activation was due to this mechanism. Lack of the precursor ^{78}Br as a stable isotope insured that the $^{79}Br^{m}$ measurement was free of slow neutron contamination. Application of the cross sections of Table I and use of Eq. (1) yielded values of $\phi(761\ keV) = (3.9 \pm 0.3) \times 10^{10}$ photons/(cm^2-keV-kRad) and $\phi(1190\ keV) = (3.4 \pm 0.9) \times 10^{10}$ photons/(cm^2-keV-kRad) for the photon flux normalized to the total delivered dose at the sample location. These values have been converted to units of MeV/(MeV-cm^2) for a particular shot so that they may be plotted in Fig.

8(a) with both the theoretical expectations for the backscattering geometry and a spectrum obtained with an absorption spectrometer.

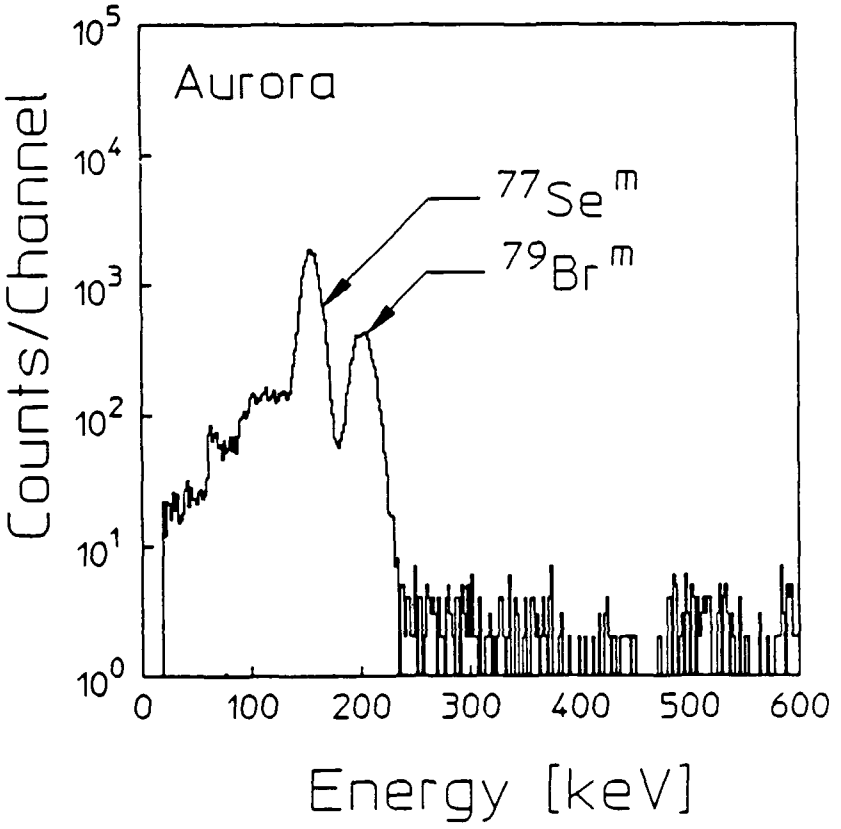

Figure 7: NaI(Tl) spectrum obtained following a single irradiation (shot 6221) at the Aurora facility in backscattered mode. Sample size is identical with that in Fig. 5. Note the difference in scale between the two figures.

As can be seen, the photoactivation measurements lie about two orders of magnitude higher than the expected values. The reason for this discrepancy lies in the high energy tail detected by the absorption spectrometer. It should be noted that although the presence of this tail is indicated by the absorption technique, the lack of sensitivity above 1 MeV in the absorption method does not permit determining the real shape of the spectrum in this region. The solid curves in Fig. 8 above about 1 MeV reflect the initial guess used in the iterative deconvolution process used for the absorption spectrometer rather than a true measurement. Separate investigations[13] of photoactivation processes in the range 1.5-6 MeV using a fixed endpoint linac designed for cancer therapy have revealed that cross sections in this interval may be

two to three orders of magnitude larger than those prevailing in the range below 1.5 MeV. Because the spectrum from the linac used in this work was fixed, it has not been possible to identify the gateway energies uniquely; thus the results have been presented in terms of possible cross section values for a single gateway state at various energies. Plots showing these single gateway cross sections versus energy are given in Fig. 9 for the four materials listed in Table I. If a gateway energy of 2.1, 3.1, 4.1, or 5.1 was assumed for either of the two materials ^{79}Br or ^{111}Cd, then the flux measurements would lie as shown in Fig 8(b). Thus, both the photoactivation measurements and the absorption spectrometer indicate the presence of a high energy tail extending above the expected backscattered spectrum. This is probably due to leakage either through the walls of the shield enclosure or around its entrance aperture.

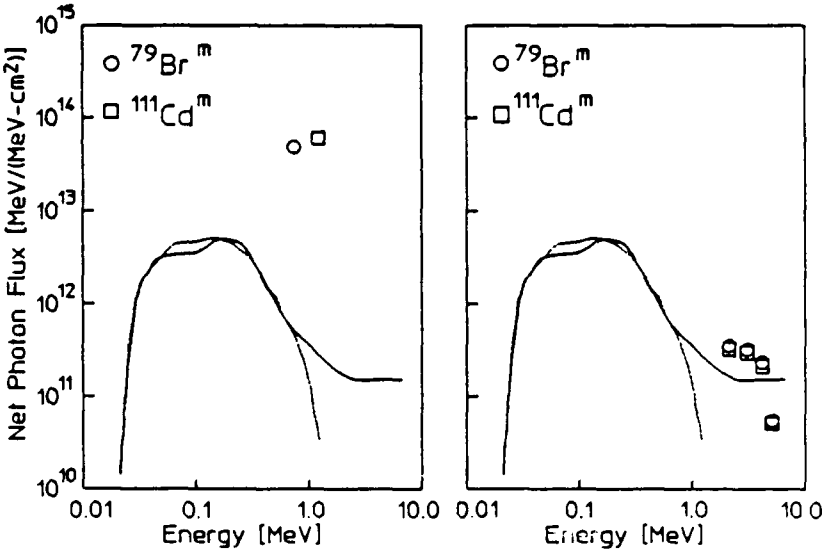

Figure 8: Comparison of photoactivation measurements in which (a) only low energy gateway states are included and (b) higher energy gateways are included. In (b) the 4 sets of points represent assumed single gateways at 2.1-, 3.1-, 4.1-, and 5.1-MeV. The dashed line is the calculated spectrum for this geometry and the solid line reflects an absorption spectrometer measurement.

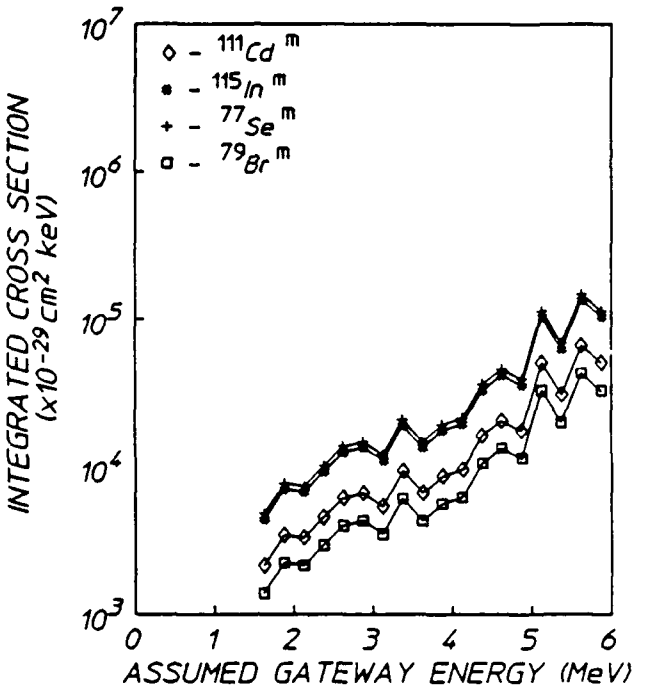

Figure 9: Possible single-gateway cross sections deduced from fixed-endpoint linac measurements.

Conclusions

Resonant nuclear photoactivation is a valuable tool that complements both more complex electronic systems and alternative activation or dosimetric methods for determining the spectrum of single-shot, intense bremsstrahlung pulses having widths of less than a microsecond. Either alone or in combination with these other methods, a properly designed photoactivation monitor package can provide the user with specific spectral intensity information on a shot-by-shot basis. Although it appears that the cross sections listed in this paper are adequate for characterizing x-ray spectra with endpoints below 1.5 MeV, additional cross section determinations for high-lying gateway states are required to extend the power of the method to higher energies.

References

1. Y. Paiss, C. D. Eberhard, and C. B. Collins, "Photonuclear Excitation for the Calibration of Pulsed Bremsstrahlung Spectra," Proof of the Feasibility of Coherent and Incoherent Schemes for Pumping a Gamma-Ray Laser, University of Texas at Dallas, Report #GRL/8702, Innovative Science and Technology Directorate of Strategic Defense Initiative Organization, September 1987, pp. 71-89.

2. D. A. Whittaker, K. G. Kerris, M. Litz, S. G. Gorbics, and N. R. Pereira, "Softening of Hard Bremsstrahlung by Compton Backscattering," J. Appl. Phys. 58, 1034-1036 (1985).

3. M. D. Goldberg and J. A. Harvey, "Neutrons," in American Institute of Physics Handbook, edited by D. E. Gray (New York: McGray Hill, 1972).

4. G. T. Baldwin and J. R. Lee, "Time Projection Compton Spectrometer (TPCS)," IEEE Trans. Nucl. Sci., NS-33, 1298-1304 (1986).

5. J. A. Anderson and C. B. Collins, "Calibration of Pulsed X-ray Spectra," Rev. Sci. Instrum. 59, 414-419 (1988), and references cited therein.

6. C. B. Collins, J. A. Anderson, Y. Paiss, C. D. Eberhard, R. J. Peterson, and W. L. Hodge, "Activation of $^{115}In^{m}$ by Single Pulses of Intense Bremsstrahlung," Phys. Rev. C 38, 1852-1856 (1988).

7. J. A. Anderson, M. J. Byrd, and C. B. Collins, "Activation of $^{111}Cd^{m}$ by Single Pulses of Intense Bremsstrahlung," Phys. Rev. C (to be published Nov. 1988).

8. E. Browne and R. B. Firestone, Table of Radioactive Isotopes, edited by V. S. Shirley, (New York: J. Wiley, 1986).

9. J. A. Halbleib and T. W. L. Sanford, "Predicted Flash X-ray Environments Using Standard Converter Configurations," Sandia Report SAND83-2572, 1983.

10. J. A. Anderson, J. M. Carroll, K. N. Taylor, J. J. Carroll, M. J. Byrd, T. W. Sinor, C. B. Collins, F. J. Agee, D. Davis, G. A. Huttlin, K. G. Kerris, M. S. Litz, D. A. Whittaker, N. R. Pereira, and S. G. Gorbics, "Nuclear Activation Techniques for Measuring Direct and Backscattered Components of Intense Bremsstrahlung Pulses," Nucl. Instrum. and Meth. (submitted).

11. "ASTM Standard Method for Determining Neutron Flux, Fluence, and Spectra by Radioactivation Techniques," Publication E 261-77, Philadelphia: American Society for Testing and Materials, 1987.

12. "ASTM Standard Method for Determining Thermal Neutron Reaction and Fluence Rates by Radioactivation Techniques," Publication E 262-86, Philadelphia: American Society for Testing and Materials, 1987.

13. J. A. Anderson, C. D. Eberhard, M. J. Byrd, J. J. Carroll, C. B. Collins, E. C. Scarbrough, and P. P. Antich, "Nuclear Photoactivation Cross Sections for Short-lived Isomeric States Excited with a 6 MeV LINAC," Nucl. Instrum. and Meth. (submitted).

THE USE OF A COMPTON SPECTROGRAPH/MONOCHROMATOR FOR THE PHOTOACTIVATION OF NUCLEI INTO METASTABLE STATES

by Y. Paiss, C. D. Eberhard, and C. B. Collins
Center for Quantum Electronics, University of Texas at Dallas

Introduction

Photoactivation of nuclei by gamma rays was reported as early as 1939.[1,2] Since then, a few tens of papers have appeared describing the $X(\gamma,\gamma')X^m$ reactions of about 20 nuclei.[3] It is assumed that one or more broad nuclear levels above the metastable level serve as gateways for the excitation, and that the contribution to the activation due to direct excitation is neglected since the width of the metastable level is extremely narrow.

In recent years, there appeared claims that part of the photoexcitation is due to a non-resonant process mediated by the K electrons around the nuclei.[4] Some papers, on the other hand, have refuted this claim by indirect measurements.[3,5]

In analogy with techniques used in atomic excitation studies, the only unequivocal investigation of the mechanism for production of metastable nuclei by gamma irradiation can be conducted through the use of a scanning monochromator. For example, ^{197}Au is easily excited by the bremsstrahlung of 3 MeV electrons into the metastable $^{197}Au^m$. Although gold has 20 known levels between the metastable level at 409 keV and 1242 keV, nothing is known of the excitation mechanism or which levels are involved, if any, within this energy range.[6]

It is the aim of this paper to describe a Compton spectrograph/monochromator (CSM) with "fast optics" to down-convert single energy gammas from a radioactive source and to use them to study the nuclear excitation function for the $X(\gamma,\gamma')X^m$ production of the metastable state. Single energy radioactive nuclei are rare. Here, this term is used for cases in which the spectrum contains only a few discrete gammas and no ambiguity occurs, e.g., ^{60}Co with two distinct energies, or ^{140}La with one dominant energy.

General Considerations

The CSM is basically a source, a scatterer, and an absorber. The source emits single energy photons of initial energy E_o which are scattered by an electron in the scatterer through a given angle, θ, and lose a portion of their energy. The new energy E, a function of the original energy, E_o, and the scattering angle θ, is given by

$$E = \frac{E_o}{1 + (E_o/mc^2)(1 - \cos\theta)} \quad , \qquad (1)$$

where mc^2 is the rest mass energy of the electron. The absorber is fabricated from the material under investigation. Upon striking it, the scattered photon is absorbed by the electrons in the sample unless the energy of the scattered photon is equal to that of a nuclear resonance transition. If this nuclear resonance transition corresponds to a gateway state connected by one or more electromagnetic transitions to the metastable state, the nuclear isomer can be formed. If the absorber is in the shape of a large foil, areas on the foil will become radioactive when they correspond to the scattering angle θ which degrades the photon energy from E_o to the resonance energy E_r. The angle θ can be measured and E_r can be estimated.

Assuming a basic configuration which is determined by the energy resolution needed with a free parameter scale length l, then:

1. For a given source, the number of photons striking the scatterer is independent of l because it depends only on the solid angle which the scatterer is presenting to the source, which is limited by the energy resolution required. (The area of the scatterer varies as l^2 and the flux density on the scatterer is proportional to the solid angle subtended by the absorber, that is as l^{-2}.)

2. For a source of a given specific activity, the source strength is proportional to the source volume, that is, varies as l^3, when self absorption effects are neglected. Thus, the total flux density on the scatterer goes as $l^3 \cdot l^{-2} = l$ and the flux density on the absorber as $l^3 l^{-2} l^3 l^{-2} = l^2$. The total number of absorbed resonance photons is proportional to the product of the flux density and the absorber area (not volume, since the

absorption depth is very shallow and is independent of l), or l^2 (flux density) $\times$ l^2 (area) = l^4. This means that the number of absorbed photons varies with the fourth power of the scale parameter. The limit on the size is governed by the absorption in the source and scatterer and by double Compton scattering.

Three forms of CSM are described with increasing complexity and efficiency.

A Single Massive Scatterer

This configuration is the basic one used by Compton himself.[7] It consists of a source, scatterer and an absorber foil as shown in Fig. 1. The part of the foil illuminated by photons scattered through angle θ which brings E to E_r will become radioactive.

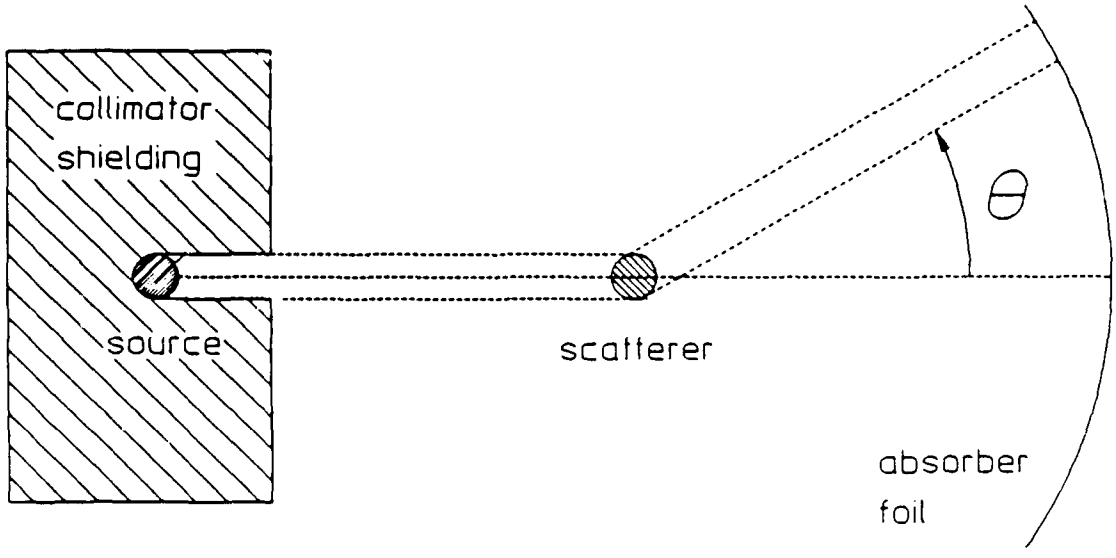

Figure 1: Geometry of the basic Compton spectrometer showing the source, single massive scatterer and a curved absorber foil.

Strip Circular Compton Spectrograph

The gamma source, the scatterer and the absorber are parts of the same circle of radius R as shown in Fig. 2. The scatterer and the absorber can be the same curved strip. All gammas scattered through the angle θ in the plane of the curve so that they strike the strip again, will arrive at the same place regardless of their scattering points on the strip (classical geometry). Therefore, they will have the same energy provided that the source is monoenergetic, such as ^{60}Co (only two lines) or ^{24}Na or ^{140}La or ^{124}Sb etc. and the photons are scattered only once.

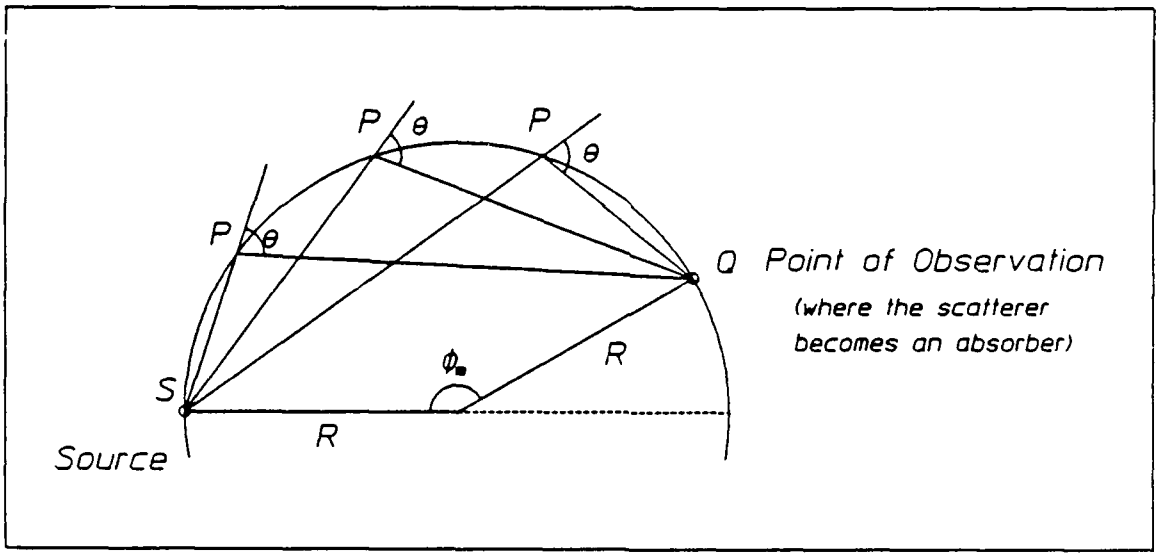

Figure 2: Compton spectrograph with curved scatterer/absorber. The curved scatterer/absorber is a section of a right-circular cylinder of radius R and height W. If the source may be considered a point source, then the angle θ is the same for all single scattering paths ending on the point Q and does not depend on the coordinates of the scattering point P. The angle θ depends only on the relative coordinates of the source S and the point of observation Q and is given by $\theta = u_m/2$.

If the energy of the photons, after being scattered through an angle θ, changes from E_o to E_r, which is the resonance energy for a nuclear absorption transition resulting in the production of an isomeric state, then after the irradiation, the strip can be autoradiographed. If the isomer formed has a sufficiently long half-life, the area on the strip corresponding to scattering through the angle θ will be radioac-

tive. The remainder of the strip, although irradiated by direct gamma from the source, will stay "cold" with a general background activation caused by Compton scattering inside the source, construction material, shielding and air, or by double scattering in the strip.

Fig. 3 indicates the angles inherent in the geometry in the circular strip scatterer. The source is located at S which corresponds to $\phi = 0$, the scattering point P at $\phi = \phi$ (arbitrary on the curve), and the absorbing point Q at $\phi = \phi_m$. The scattering point P is characterized by the angle ϕ, the P-Q distance $R'(\phi)$, and the S-P distance $R''(\phi)$. The S-Q distance is L. The scattering angle is given by $\theta = \phi_m/2$ for all scattering points on the arc of the circle of radius R. The width and thickness of the foil are given by W and D, respectively. The electron density in the foil is η. It is assumed that the mean free path of the photon of energy E_o is greater than D/sin (ϕ/2) which is the maximum slant range of a photon inside the foil.

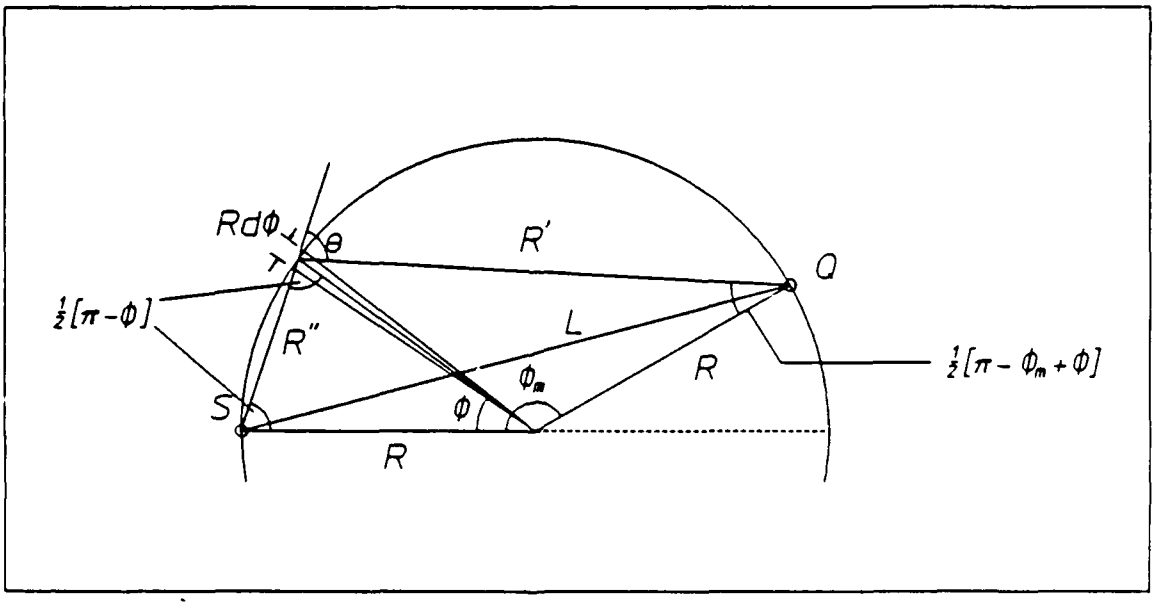

Figure 3: Compton spectrograph with curved scatterer/absorber showing the geometrical details employed in the calculations. From this, the following definitions are easily seen:

$R' = 2\ R \sin [(\phi_m - \phi)/2]$
$R'' = 2\ R \sin (\phi/2)$
$L = 2\ R \sin (\phi_m/2) = 2\ R \sin \theta$

There is a one-to-one correspondence between the scattering angle θ and the energy of the scattered photon E when a monoenergetic source is used. The scattering efficiency of an electron is determined by the Kline-Nishina cross section σ_C. By integrating it over the azimuthal scattering angle and substituting dependence on E for the dependence on θ, the following expression[8] can be used to determine the cross section for the scattering of a photon of initial energy E_o into the energy interval $E_r \pm \Gamma/2$ of the nuclear resonant absorption transition at E_r:

$$\sigma(E_r,E_o) = \int_{E_r-\Gamma/2}^{E_r+\Gamma/2} \sigma(E,E_o)\, dE \simeq \sigma_C(E_r,E_o)\,\Gamma \qquad (2)$$

$$= \pi r_o^2 \frac{mc^2\Gamma}{E_o^2}\left[\frac{E_o}{E_r} + \frac{E_r}{E_o} + \left(\frac{mc^2}{E_r} - \frac{mc^2}{E_o}\right)^2 - 2mc^2\left(\frac{1}{E_r} - \frac{1}{E_o}\right)\right] .$$

where $r_o = e^2/mc^2$ is the classical radius of the electron and E_r may range from a minimum of $E_o/(1 + 2E_o/mc^2)$ for $\theta = \pi$ (backscattering) to E_o for $\theta = 0$ (no scattering).

The total number of scattering events in the differential volume dV at P which produce photons of energies in the interval $E_r \pm \Gamma/2$ is given by

$$dn(E_r) = \eta\, \sigma(E_r,E_o)\, \Phi(P)\, dV \qquad (3)$$

$$= \eta\, \sigma(E_r,E_o)\, \frac{1}{4\pi(2R \sin \phi/2)^2}\, W\, D\, R\, d\phi \quad ,$$

where $\sigma(E_r,E_o)$ is the cross section as defined above, η is the electron density, and $\Phi(P)$ is the flux of monoenergetic photons produced by the radioactive source S (which is assumed to be isotropic and normalized to one disintegration/sec).

The differential increment of the spectral density at Q, $d\psi$, is defined as follows: the number of photons per unit area per unit time at Q with energies in the interval $E_r \pm \Gamma/2$ produced by Compton scattering in the volume dV at P per unit energy interval per Bq. This differential increment is given by

$$d\psi = [dn(E_r)/\Gamma] \cdot \sin\frac{\phi_m-\phi}{2} \cdot [1/2\pi R' \sin\theta] \cdot [1/g] \quad . (4)$$

The first multiplicative factor corrects for the oblique incidence of the scattered photons on the absorber at Q. The second factor represents the percentage of the total scattered flux intercepted by the absorber (σ_c has already been integrated azimuthally in Heitler's expression) and finally g is the width of the active line formed on the absorber. It is larger than the width dictated by the level width of the absorber, and we assume it to be the image of the source on the absorber. In our geometry, the magnification is unity.

Integration over the angle ϕ from the minimum ϕ_o to ϕ_m yields the total Compton scattered flux with energy in the interval $E_r \pm \Gamma/2$ at the point of activation Q,

$$\psi = \int_{\phi_o}^{\phi_m} \frac{\eta WDR d\phi \sigma_c(E_r, E_o)}{16\pi R^2 \sin^2(\phi/2)} \cdot \frac{\sin\frac{\phi_m-\phi}{2}\ \frac{1}{g}}{2\pi\ 2R \sin\frac{\phi_m-\phi}{2} \sin\theta} \qquad (5)$$

$$= K\int_{\phi_o}^{\phi_m} \frac{d\phi}{\sin^2(\phi/2)} = 2K[\cot(\phi_o/2) - \cot(\phi_m/2)] \quad ,$$

where $K = [\eta WD\sigma_c/(8\pi R)^2 \sin\theta\ g]$ and ϕ_o is the minimum ϕ corresponding to the closest edge of the scattered/absorber outside the source volume.

Equation (5) may be rewritten as

$$\psi = 2K \frac{\sin\frac{\phi_m-\phi_o}{2}}{\sin(\phi_m/2) \sin(\phi_o/2)} \qquad (6)$$

This expression becomes infinite as ϕ_o approaches zero, so that we must look more closely to discover the limitation of our geometry and the restraints on ϕ_o.

The original diverging term arises from the description of the source as a point source,

$$\Phi = \frac{1}{4\pi r^2} = \frac{1}{4\pi\ [2R \sin \phi/2]^2} \quad , \tag{7}$$

where ϕ describes the point of observation on the arc. As one approaches the point source, $\phi \to 0$, $r \to 0$ and $\Phi \to \infty$. In reality, the source has a finite size and the flux is integrated over a sphere outside the source. If the minimum size of this sphere is $r = 2R \sin (\phi_o/2)$, then the minimum ϕ could be found from this.

A second concern is that in the usual planar scattering geometry, the effective thickness $(D/\sin [\phi/2])$ as expressed in our geometry becomes infinite as $\phi \to 0$ which corresponds to the beam becoming parallel to the surface. For a spherical shell or a narrow circular strip, the maximum effective thickness is given by $[D(2R+D)]^{1/2}$. So one must impose the condition on ϕ_o that

$$\frac{D}{\sin \phi_o/2} << [D(2R+D)]^{1/2} \quad , \tag{8}$$

which should be fulfilled also to prevent double Compton scattering. This is equivalent to moving the edge of the scatterer far enough away that the spherical shell can be approximated by the planar sheet.

As shown in Fig. 3, the dependence of the flux on ϕ_o may also be expressed as

$$\psi(\phi_o) = \frac{\eta\ WD\ \sigma_C}{8\pi^2\ g} \frac{R'(\phi_o)}{L^2\ R''(\phi_o)} \tag{9}$$

$$\simeq \frac{\eta\ WD\ \sigma_C}{8\pi^2\ g} \frac{1}{R''(\phi_o)\ L} \quad ,$$

when $R'(\phi_o) \simeq L$, which implies that ϕ_o is very small.

Let us assume that the same parameters (n, D , W, etc.) describe both the massive scatterer and the extended scatterer (strip). Now as shown in Fig. 4, let us consider the massive scatterer to be the beginning segment of the extensive one (strip).

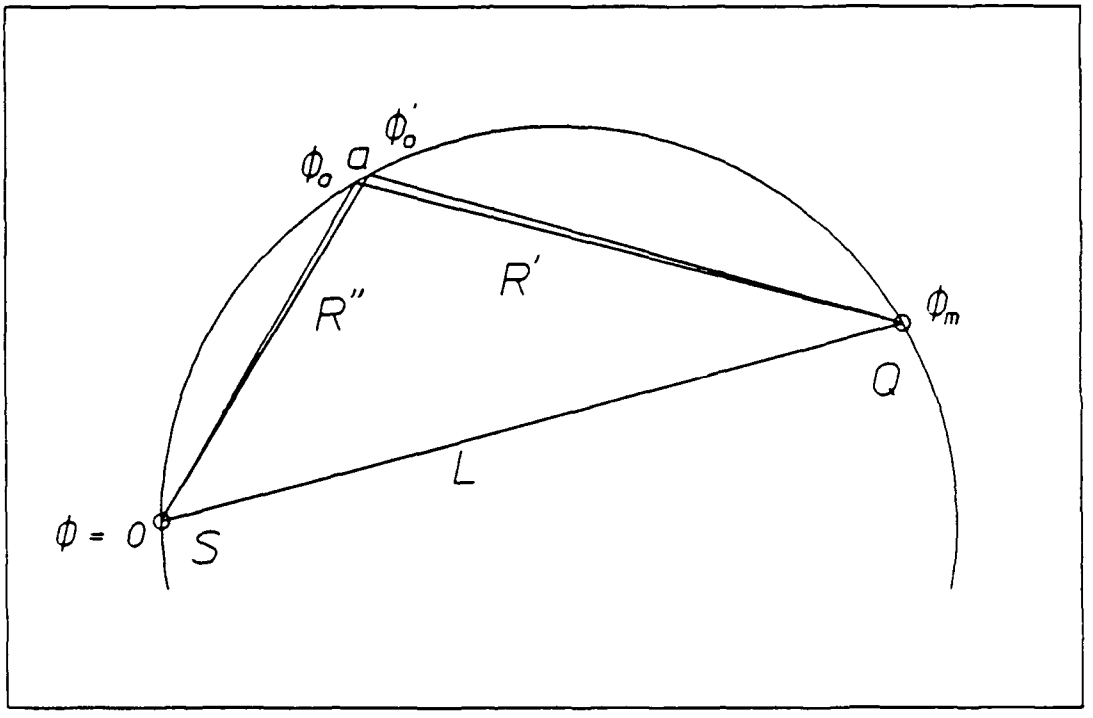

Figure 4: Compton spectrograph with curved scatterer/absorber with geometrical details for the comparison of the extended strip scatterer with the single massive scatterer.

Its contribution is the difference between that of an extensive scatterer from ϕ_o to ϕ_m to that from ϕ_o' to ϕ_m,

$$\psi_{massive} = \psi(\phi_o) - \psi(\phi_o') \tag{10}$$
$$= \frac{\eta \text{ WD } \sigma_c \left[\cot(\phi_o/2) - \cot(\phi_o'/2)\right]}{32\pi^2 R^2 \sin\theta \text{ g}}$$
$$= \frac{\eta WD\sigma_c}{32\pi^2 R^2 \sin\theta \text{ g}} \quad \frac{\sin([\phi_o'-\phi_o]/2)}{\sin(\phi_o'/2)\sin(\phi_o/2)}$$

Thus the ratio is given by

$$\frac{\psi_{massive}}{\psi_{strip}} = \frac{\sin([\phi_o'-\phi_o]/2)\sin(\phi_m/2)}{\sin(\phi_o'/2)\sin([\phi_m-\phi_o]/2)} \tag{11}$$
$$\simeq \frac{aL}{R''(\phi_o')R'(\phi_o)} .$$

As shown in Eq. (9), $\psi(\phi_o)$ is greater when $R''(\phi_o) < R'(\phi_o)$. Therefore, in an optimal strip, $R'(\phi_o) \simeq L$ and Eq. (11) can be written

$$\frac{\psi_{massive}}{\psi(\phi)} \simeq \frac{a}{R''(\phi_o)} . \tag{12}$$

To estimate the maximum value of the parameter a which characterizes the size of the scatterer, let us consider the massive scatterer to be a ball with the diameter a, situated such that $R'(\phi_o) = R''(\phi_o)$. Figure 5 shows this arrangement.

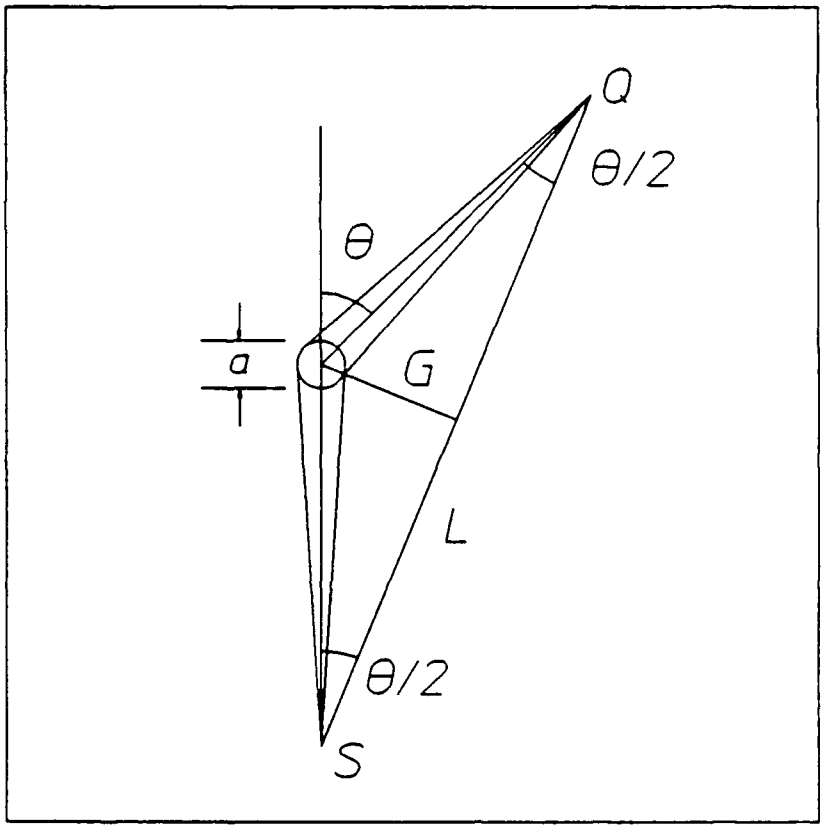

Figure 5: Geometrical details for the estimate of maximum size of a single massive spherical scatterer for a given energy spread.

By simple trigonometry,

$$G = \frac{L}{2} \tan(\theta/2) = \frac{L}{2} \frac{1 - \cos\theta}{\sin\theta} , \qquad (13)$$

and the energy E of the Compton scattered photon may be rewritten as

$$E = \frac{mc^2}{1 - \cos\theta + (mc^2/E_o)} . \qquad (14)$$

A change of the scattering point along G will change the energy of the scattered photon E as

$$\frac{dE}{dG} = \frac{dE}{d\theta}\frac{d\theta}{dG} = \frac{-mc^2 \sin\theta}{[1 - \cos\theta + (mc^2/E_o)]^2} \frac{2}{L} \frac{\sin^2\theta}{(1 - \cos\theta)} , \qquad (15)$$

or

$$-\frac{dE}{dG} = \frac{E^2}{mc^2}\frac{\sin^2\theta}{G} \quad , \tag{16}$$

by the substitution of (13) and (14) in (15). Now assuming $(a/2) \ll G$, the change in energy of the scattered photon from the most remote part of the ball along G, $\Delta G = a/2$, is given by

$$\Delta E = \frac{dE}{dG}\Delta G = \frac{E^2}{mc^2}\frac{a}{2G}\sin^2\theta \quad . \tag{17}$$

For example, to reduce the 1.33 MeV gamma from ^{60}Co to 1 MeV, the scattering angle θ is about 29°, so that

$$\Delta E \simeq \frac{(1.0)^2}{(0.51)}\frac{a}{2G}\sin^2 29° = \frac{(0.461)(a/2)}{G} \quad . \tag{18}$$

If a 5% maximum spread in energy E is desired, then Eq. (17) is

$$\frac{\Delta E}{E} = \frac{E}{mc^2}\frac{(a/2)}{G}\sin^2\theta \tag{19}$$

$$= \frac{(1.0)}{(0.51)}\frac{(a/2)}{G}(0.235) = 0.05 \quad .$$

Solving for the radius of the ball, (a/2), we have

$$(a/2) = (0.05)(2.17)\,G = 0.11\,G \quad . \tag{20}$$

Typically, experimental parameters would be $R'' \simeq R' \simeq 30$ cm, $G = R''\sin(\theta/2) \simeq 7.5$ cm and $(a/2) \simeq 0.8$ cm. Substituting this into Eq. (11), we get

$$\frac{\psi_{massive}}{\psi_{strip}} = \frac{(1.6)(58)}{(30)(30)} = 0.11 \quad . \tag{21}$$

The strip then is about an order of magnitude more efficient than the massive scatterer.

The Football Geometry Compton Spectrograph

By rotating the strip around L as an axis, one obtains a football shaped scattering surface for $\theta < \pi/2$. For $\theta = \pi/2$, the shape is a sphere and for $\theta > \pi/2$, it is a donut with a clogged hole. Here we shall limit our discussion only to the football shape because $\theta \geq \pi/2$ will seldom be used.

The source is located at one apex of the football and the absorber at the other apex of the scatterer as shown in Fig. 6.

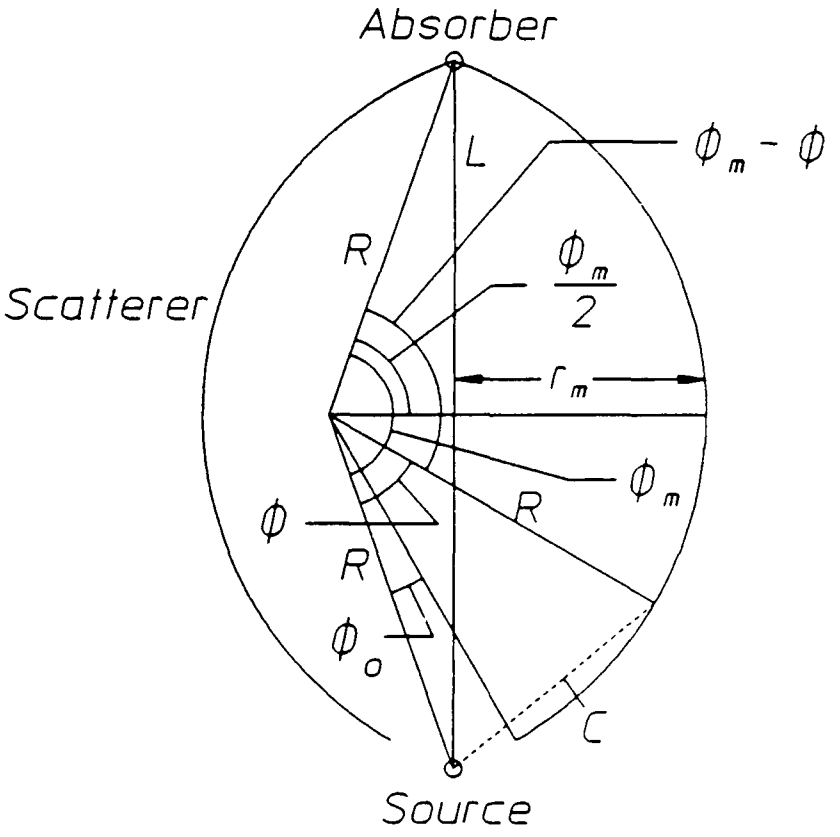

Figure 6: "Football-shaped" spectrometer utilizing the curved scatterer/absorber concept. From this, the following definitions used in the calculation may be seen:

$\sin(\phi_m/2) = L/2R$; $1 - \cos(\phi_m/2) = r_m/R$

$\sin(\phi_i/2) \simeq \phi_i/2$; $1 - \cos(\phi_i/2) \simeq \phi_i^2/4$

$c = 2R \sin(\phi/2)$

$r = c \sin[(\phi_m - \phi)/2] = 2R \sin(\phi/2) \sin[(\phi_m - \phi)/2]$

To calculate the flux density on the absorber, we can use an equation similar to Eq. (5), replacing the strip width W by the length of the circumference at latitude ϕ on the ball,

$$W = 2\pi r = 4\pi R \sin(\phi/2) \sin([\phi_m-\phi]/2) \quad . \tag{22}$$

Another change from Eq. (5) is the omission of the sin $([\phi_m-\phi]/2)$ in the numerator. This arises because the absorber is no longer a part of the scatterer, but a plug at the top of the ball. The gammas strike the absorber practically normal to the surface and no correction for the slant angle is needed. With these modifications, Eq. (5) becomes

$$\psi = \int_{\phi_o}^{\phi_m} \frac{\eta D[4\pi R \sin(\phi/2) \sin((\phi_m-\phi)/2)] R \sigma_c \, d\phi}{16\pi R^2 \sin^2(\phi/2) \, 4\pi R \sin((\phi_m-\phi)/2) \sin\theta \, g} \tag{23}$$

$$= \frac{\eta\sigma_c D}{8\pi R g \sin\theta} \log\left[\frac{(1-\cos(\phi_m/2))}{\sin(\phi_m/2)} \frac{\sin(\phi_o/2)}{(1-\cos(\phi_o/2))}\right] .$$

Referring to Fig. 6, we may rewrite this for small values of ϕ_o as

$$\psi = \frac{\eta\sigma_c D}{8\pi R g \sin\theta} \log \frac{2r_m/L}{\phi_o/4} \quad , \tag{24}$$

where r_m is the distance $R[1-\cos(\phi_m/2)]$.

By dividing Eq. (24) by Eq. (9), we get the relative efficiency of the football to the strip configuration,

$$\frac{\psi_{football}}{\psi_{strip}} = \frac{2\pi R''(\phi_o) L \log[(2r_m/L)/(\phi_o/4)]}{WR'(\phi_o)} \tag{25}$$

$$\simeq \frac{2\pi R''(\phi_o) \log[(2r_m/L)/(\phi_o/4)]}{W} \quad ,$$

since $R'(\phi_o) \simeq L$. The quantity $\log[(2r_m/L)/(\phi_o/4)]$ is on the order of 2 to 5 in our geometry. The quantity $R'(\phi_o)/W$ is of the order of 5. The relative efficiency is therefore on the order of 60 to 160, or, about two orders of magnitude more than that of a simple solid scatterer.

Let us consider an example case in which the scatterer and absorber have the following parameters:

$\sigma_c = 1.7 \times 10^{-28}$ cm^2 (Klein-Nishina cross section[8] for scattering a 1.3 MeV photon to 1 MeV) ,

$R = 100$ cm ,

$\theta = 29°$,

g = the source radius $= 1$ cm ,

$D = 0.3$ cm ,

$\log [(2r_m/L)/(\phi_o/4)] = 4$, and

$\eta \approx 1.9 \times 10^{24}$ cm^{-3} (typical value for In) .

The normal component of the flux at the absorber calculated from Eq. (24) is

$$\psi = 9.7 \times 10^{-7} \text{ photons/cm}^2 \text{ sec keV Bq} \quad . \qquad (26)$$

Therefore, a 6 kilocurie ^{60}Co source will deliver a 1 MeV photon flux of 2.2×10^8 photons/cm^2 sec keV to the absorber. These are the 1.33 MeV photons scattered through an angle of 29°.

Discussion

We see that the "football-shaped" scatterer can serve as a monochromator for the production of gamma rays with an energy range between the maximum energy of the available gamma sources and those energies obtained by the crystal diffraction methods. Although the football has relatively "slow optics," it is the best tunable gamma source available. One drawback is that by contrast to the strip CSM, the football lacks continuous tunability. For each source-absorber combination, a different arc of the scatterer must be used for each value of energy. We should investigate the potential for continuous tuning by inflating a uniform, expandable ball or by constructing the scatterer from elastic ribs which can be adjusted at the poles. Care must be taken to insure a circular configuration, perhaps by varying the thickness of the substrate material holding the scatterer.

A fast shuttle between the ball's apex and a shielded detector would enable the determination of gateway levels of isomers with half-lives down to a second. With high specific activity sources (e.g., ^{140}La) and optimization (no attempt to optimize was done in the example given) of the CSM by ray tracing and Monte Carlo calculations, we hope to increase the flux by at least an order of magnitude.

References

1. B. Pontecorvo and A. Lazard, C. R. Acad. Sci. 208, 99 (1939).

2. G. B. Collins, B. Waldman, E. M. Stubblefield, and M. Goldhaber, Phys. Rev. 55, 507 (1939).

3. K. Yoshihara, Zs. Nemeth, L. Lakosi, I. Pavlicsik, and A. Veres, Phys. Rev. C33, 728 (1986) contains a thorough review.

4. A. Ljubicic, K. Pisk, and B. A. Logan, Phys. Rev. C23, 2238 (1981).

5. C. B. Collins, J. A. Anderson, Y. Paiss, C. D. Eberhard, R. J. Peterson, and W. L. Hoddge, Report GRL/8702, 45 (1987).

6. B. Harmatz, Mucl. Data Sheets 34, 101 (1981).

7. A. H. Compton and S. K. Allison, X-rays in Theory and Experiment, (D. Van Nostrand Co., Inc., New York, 1935).

8. W. Heitler, The Quantum Theory of Radiation, (Oxford University Press, London 1944).